

Thermal Degradation of Electroplated Nickel Thermal Microactuators

J. K. Luo, Y. Q. Fu, J. A. Williams, and W. I. Milne

Abstract—In this paper, the thermal degradation of laterally operating thermal actuators made from electroplated nickel has been studied. The actuators investigated delivered a maximum displacement of ca. 20 μm at an average temperature of $\sim 450^\circ\text{C}$, which is much lower than that of typical silicon-based microactuators. However, the magnitude of the displacement strongly depended on the frequency and voltage amplitude of the pulse signal applied. Back bending was observed at maximum temperatures as low as 240°C . Both forward and backward displacements grew as the applied power was increased up to a value of 60 mW; further increases led to reductions in the magnitudes of both displacements. Scanning electron microscopy clearly showed that the nickel beams began to deform and change their shape at this critical power level. Compressive stress is responsible for nickel pileup, while tensile stresses, generated upon removing the current, are responsible for necking at the hottest section of the hot arm of the device. Energy dispersive X-ray diffraction analysis also revealed the severe oxidation of Ni structure induced by Joule heating. The combination of plastic deformation and oxidation was responsible for the observed thermal degradation. Results indicate that nickel thermal microactuators should be operated below 200°C to avoid thermal degradation. [2009-0015]

Index Terms—Back bending, electroplating, oxidation, plastic deformation, thermal actuator, thermal degradation.

I. INTRODUCTION

THE ATTRACTION of microelectrothermal actuators for use in microsystems and microelectronics lies in the relatively large forces and displacements which they can generate [1]–[3]. With operational voltages comparable to those used in CMOS, they are particularly suitable for integration with electronic circuits for control and signal processing. In general, microactuators have longer lifetimes than their macro counterparts, owing to the reduced number of defects in components with such small linear dimensions. The operational durability and reliability of microactuators are thus generally superior

Manuscript received January 15, 2009; revised September 15, 2009. The work of J. K. Luo was supported in part by the Engineering and Physical Sciences Research Council under Project EP/D051266. Subject Editor M. Wong.

J. K. Luo is with the Engineering Department, University of Cambridge, Cambridge, CB3 0FA, U.K., and also with the Centre for Material Research and Innovation, University of Bolton, Bolton, BL3 5AB, U.K. (e-mail: j2.bolton.ac.uk.).

Y. Q. Fu is with the Engineering Department, University of Cambridge, Cambridge, CB3 0FA, U.K., and also with the Department of Mechanical Engineering, School of Engineering and Physical Sciences, Heriot Watt University, Edinburgh, EH14 4AS, U.K.

J. A. Williams and W. I. Milne are with the Engineering Department, University of Cambridge, Cambridge, CB3 0FA, U.K.

Color versions of one or more of the figures in this paper are available online at <http://ieeexplore.ieee.org>.

Digital Object Identifier 10.1109/JMEMS.2009.2034394

to macroactuators. Microelectromechanical system (MEMS) switches and comb-drive structures based on electrostatic actuation have been operated up to tens of billion of cycles without failure [4]. However, thermal microactuators have shorter lifetimes, particularly when operated at high temperatures. When operated in these conditions, deterioration in actuation force and actuation frequency, as well as degradation in maximum displacement and catastrophic failure by burn-off or blowup, has been reported for both lateral and vertical thermal microactuators [5], [6]. Thermal degradation is attributable to both surface oxidation and plastic deformation caused by material creep at elevated temperatures. When a thermal microactuator is heated above some critical temperature, it may undergo localized material deformation, oxidation, creep, or even recrystallization in the most vulnerable position [5], [6]. In Si-based actuators, a structural deformation phenomenon, known as “back bending,” is often observed, whereby the actuating elements will not return to their original positions once they have been “overactuated” but are left permanently bent or deformed in the direction opposite to that of normal actuation.

Plastic deformation caused by creep and recrystallization increases rapidly with temperature. For a typical lateral thermal actuator consisting of a combination of hot and cold arms, as shown in Fig. 1(a), the highest temperature occurs near the middle of the hot arm; however, the largest stress usually occurs either near the joint of the hot and cold arms or at the root of the beams or flexures which allow the structure to move. If material creep exists at a raised temperature, we should expect material pileup or accumulation to occur at the place where the compressive stress is the largest. Although there is no direct reported evidence of such compressive deformation, tensile tests of Si microbeams, at various elevated temperatures, have revealed thinning due to creep [7]. The temperature required for plastic deformation in a Si actuator is believed to be correlated with the intrinsic melting temperature ($\sim 1414^\circ\text{C}$) of this material [8]. The observed plastic deformation transition temperature for Si actuators, however, is typically $600^\circ\text{C} \sim 800^\circ\text{C}$ [6], which is much lower than the intrinsic melting temperature of silicon. It was believed that the plastic deformation of the silicon actuators is dominated by brittle-to-ductile transition temperature which is $\sim 660^\circ\text{C}$ [9], which is within the observed plastic deformation transition temperatures ($600^\circ\text{C} \sim 800^\circ\text{C}$) for silicon thermal actuators. Although thermal degradation has been studied in microactuators for many years [5]–[11], the degradation mechanisms are still not clear.

Silicon is the dominant material used for MEMS devices not least because of the suite of microfabrication technologies and

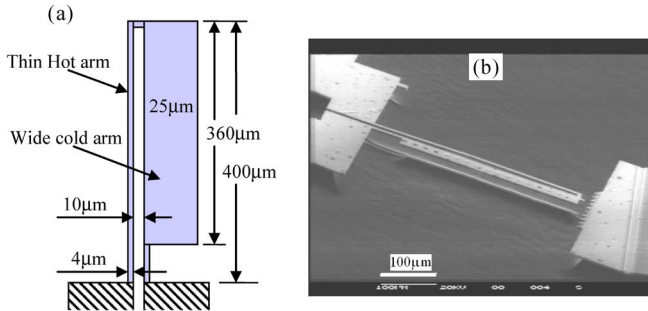


Fig. 1. (a) Schematic drawing of the U-shaped thermal microactuator. (b) SEM photograph of the U-shaped Ni thermal microactuator.

87 manufacturing facilities inherited from the microelectronics
88 industry. Since metals have higher thermal expansion coeffi-
89 cients than silicon, metallic thermal microactuators have lower
90 operation temperatures. For example, if a Si actuator needs an
91 operation temperature around 1000 °C to deliver a particular
92 displacement, then a Ni-based actuator would only require a
93 temperature of ~400 °C [12]. In addition, nickel-based actua-
94 tors have much lower resistivity and are thus particularly suit-
95 able for microactuator-based microrelays and microswitches
96 [13], [14].

97 Nickel and Ni-Fe alloys are the most studied metals for
98 microactuators because of their attractive material properties
99 and easy fabrication by electroplating [12], [13]. Although
100 nickel has a high melting temperature (1455 °C), which is
101 higher than that of silicon (1414 °C), it is ductile in nature.
102 Metals oxidize at much lower temperatures than silicon, and
103 thus, the temperature limitation of a metal device is expected to
104 be much lower than its silicon counterpart. Indeed, a limiting
105 temperature of ~200 °C has been suggested for the nickel ther-
106 mal actuators, although with little experimental support [15].
107 The degradation of electrodeposited Ni structures and devices
108 has been studied under high stress by many groups, [16]–[18]
109 but mostly at room temperatures. There is a lack of studies on
110 Ni microstructures and devices under thermal stress. This paper
111 reports a systematic investigation on the thermal degradation of
112 a nickel thermal microactuator, including back bending, creep,
113 and oxidation.

114 II. FABRICATION AND ELECTRICAL TESTING

115 Fig. 1(a) shows a schematic drawing of the U-shaped lateral
116 thermal actuators used for this investigation. Each device con-
117 sisted of a thin hot arm and a wider cold arm joined by a thin
118 flexure. All the U-shaped actuators used in this paper had the
119 same dimensions. The length and width of the hot arms were
120 400 and 4 μm, respectively, with the corresponding dimensions
121 of the cold arms being 360 and 25 μm. The flexure at the
122 base of the cold arm was 40 μm long and 4 μm wide, and
123 the gap between the hot and cold arms was 10 μm. When a
124 current passes through a resistive device, its temperature rises
125 through Joule heating. In the case of a thermoelectric actuator,
126 the higher electrical resistance of the thinner beam leads to its
127 reaching a much higher temperature than the cold arm. This, in
128 turn, generates a greater change in length by thermal expansion,

thus producing a deflection of the free tip laterally toward the
cold arm.

The microactuators used in this paper were made from elec-
troplated nickel films using a through-mask-plating technology
[19], [20]. The devices were fabricated using a single-mask
process on a 4-in Si wafer: The details of the process can be
found in [12] and [21]. The thicknesses of the nickel films
for two batches of devices, designated hereafter as D1 and
D2, were 3 and 4 μm, respectively. The devices were released
by etching the Si underneath the nickel beams using a SF₆
reactive ion etch process. The plasma etching conditions were
as follows: a SF₆ flow rate of 45 sccm, a pressure of 150 mtorr,
an RF power of 150 W, and an etch time of 15 min. The
etch duration was long enough to remove all residual silicon
from the back of the devices which were separated from the
Si substrate by an air gap of 25–30 μm, which is sufficient
to minimize conductive losses. Fig. 1(b) shows a scanning
electron microscopy (SEM) of the D2 nickel microactuator with
a Ni thickness of ~4 μm. The surfaces of the devices were
smooth with a typical roughness of less than 20 nm, and the
sidewalls were almost vertical.

Electrical tests were conducted on the actuators using a probe
station. The motion of the actuators was captured by a video
camera with a resolution of 0.5 μm and was subsequently
analyzed by a commercial software. The actuators were driven
by a pulsed current using a Keithley voltage source Type 224,
which simultaneously monitored the voltage drop across the
devices, so that the power consumption and resistance of the
actuator could be calculated. A rising temperature will increase
the electrical resistance of the device due to the positive tem-
perature coefficient of the resistivity of metals. The average
temperature change of the thermal microactuator ΔT_{ave} can be
extracted from the change of the resistance by the relation [22]

$$\Delta T_{ave} = T - T_0 = (R(T) - R_0) / R_0 \xi \quad (1)$$

where T_0 is the room temperature, R_0 and $R(T)$ are the re-
sistances of the device at room temperature and the raised tem-
perature, respectively, and ξ is the temperature coefficient of the
resistivity of the Ni with a value of $3 \times 10^{-3} \text{ K}^{-1}$ obtained from
our previous work [23]. A metal such as nickel can be easily
oxidized at high temperatures, so that the resistance of the actu-
ator will increase during high-temperature measurements. This
may cause an underestimation of the device temperature. Since
significant metal oxidation occurs at temperatures $> 450^\circ\text{C}$,
except for those specific experiments observing the enhanced
deformation and oxidation processes, pulsed low currents were
used for the measurements to keep the surface temperature of
the beams at levels at which oxidation would be minimal.

The off-power tip position of a microactuator may gradually
shift due to the so-called back-bending effect, and the resistance
may also change after each measurement. In order to deter-
mine an accurate tip forward displacement and a back-bending
displacement, it was necessary to measure both the off-power
tip position (i.e., the back bent position) and resistance be-
fore starting each measurement. The measurement procedures
were as follows: 1) Measure the off-power position and resis-
tance; 2) apply a pulse current; 3) measure the corresponding

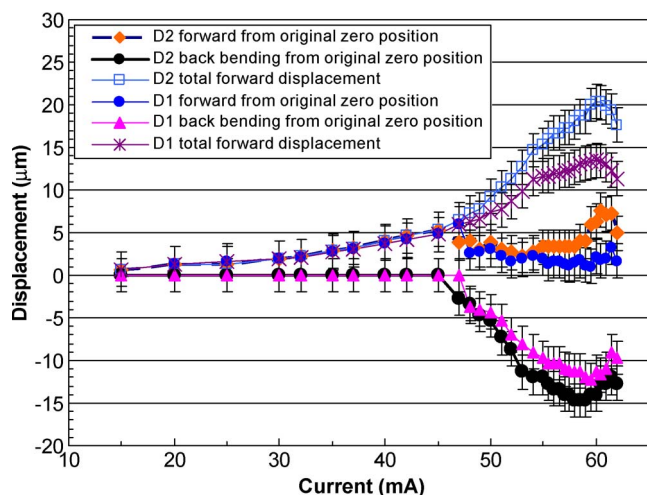


Fig. 2. Displacements of the Ni actuators as a function of pulsed current. The current pulsewidth was 0.1 s. Device D1 and D2 have different Ni thicknesses of 3 and 4 μm .

184 displacement and the voltage drop for resistance and power
 185 calculations; 4) turn off the current; and 5) remeasure the
 186 off-power position and resistance as part of the next measure-
 187 ment sequence. Metals have a positive temperature coefficient
 188 of resistivity, so that if the cooling of the hot arm is insufficient,
 189 then this element of positive feedback can lead to thermal run-
 190 away and structural failure. For the majority of the experiments,
 191 the current pulse duration was therefore limited to 0.1 s to
 192 avoid overheating and thermal destruction. However, in order
 193 to investigate the deformation and oxidation of the nickel beam
 194 that can occur in extreme circumstances, some experiments
 195 were carried out in which a current sufficient to generate the
 196 largest displacement of the actuator was applied to the actuator
 197 for a duration of 3 min. The subsequent surface morphology
 198 of the Ni beams was then characterized using field emission
 199 SEM (JEOL 6340F). Elemental concentrations at the surfaces
 200 of the nickel beams were measured using an energy dispersive
 201 X-ray (EDX) analyzer. The bonded oxygen content in the NiO_2
 202 formed during operation could be calculated from the intensity
 203 of the EDX curves.

204 III. RESULTS AND DISCUSSIONS

205 A. Displacement Versus Power

206 Two nickel thermal actuators D1 and D2 with nickel film
 207 thicknesses of 3 and 4 μm , respectively, were studied. Fig. 2
 208 shows the observed displacement from the original zero posi-
 209 tion, back bending, and the total forward displacement, which is
 210 the sum of the former two, with current as input variable. Fig. 3
 211 shows the back bending and the total forward displacement as
 212 a function of power calculated using the current applied and
 213 the resistance measured. The back-bending displacements were
 214 measured from the original zero position, and the minus sign
 215 represents its displacement opposite to the forward displace-
 216 ment. The total forward displacements (forward displacement
 217 in short hereinafter) of the thermal microactuator tips increased
 218 parabolically with the current applied and, up to an input of
 219 60 mW, were roughly proportional to the applied power, in

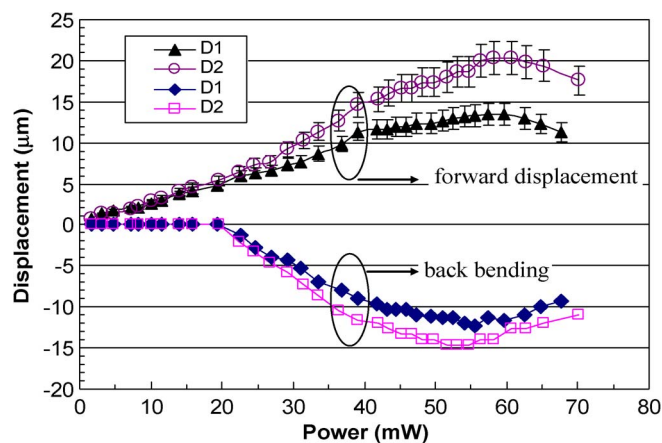


Fig. 3. Forward displacements and back bending of the Ni actuators as a function of power consumed, which were calculated from the current applied and voltage measured. The back bending appears at a current larger than 20 mA.

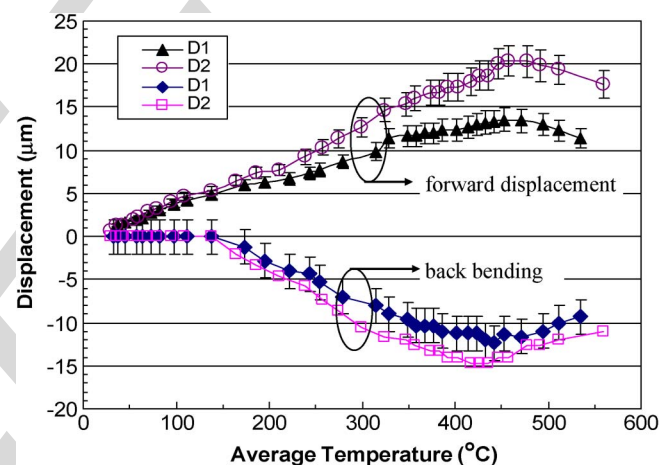


Fig. 4. Forward displacements and back bending as a function of average temperature extracted for two thermal actuators. The forward displacement is almost proportional to the average temperature. The back bending appears at an average temperature larger than 140 $^{\circ}\text{C}$.

220 agreement with theoretical analysis in the literature [12], [22].
 221 For both D1 and D2, the displacement of the tip reached a 221
 222 maximum at a power of 60 mW, specifically at values of 222
 223 ~ 16 and 20 μm , respectively; beyond this, the displacement 223
 224 decreased with any further increase in power due to thermal 224
 225 degradation, as discussed later. 225

226 The observed forward displacement and back bending of the 226
 227 microactuators D1 and D2 are shown in Fig. 4 as a function of 227
 228 their average temperatures calculated by (1). The displacement 228
 229 is approximately proportional to the average temperature up 229
 230 to a value of 450 $^{\circ}\text{C}$, above which the displacement decreases: 230
 231 This may well be due to thermal degradation, as discussed 231
 232 later. For a similar displacement, a Si-based thermal actuator 232
 233 would typically require an average temperature of over 1000 $^{\circ}\text{C}$ 233
 234 [4], [5]. The much lower operating temperatures of nickel 234
 235 actuators are attributable to their larger thermal expansion 235
 236 coefficient $\alpha = 15 \times 10^{-6} \text{ K}^{-1}$ compared to that of silicon for 236
 237 which $\alpha = 2.5 \times 10^{-6} \text{ K}^{-1}$. 237

238 The reported tip displacement for U-shaped actuators is 238
 239 typically $\sim 5\%$ of the length of the hot arm [5]. The observed 239

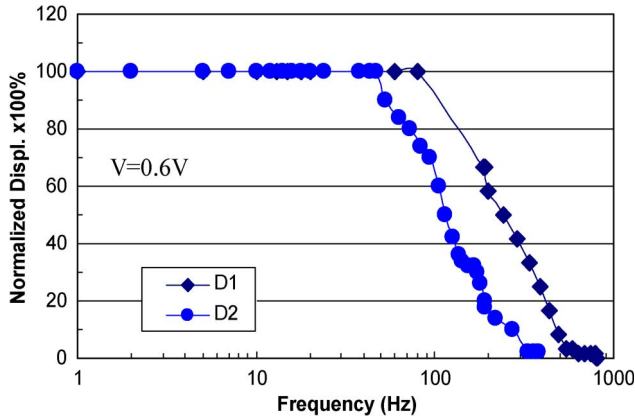


Fig. 5. Dependence of normalized displacements of Ni actuators on the frequency. The displacement remains unchanged at a frequency smaller than 40–100 Hz; it decreases with increasing the frequency and diminishes at a frequency higher than 300–700 Hz.

240 displacement of $\sim 20 \mu\text{m}$ for nickel devices with a length of
 241 $400 \mu\text{m}$ is therefore comparable to those reported for silicon
 242 actuators [1], [5] but occurs at a much low operating tempera-
 243 ture. Further reductions in the temperature required or increases
 244 in the displacements of the tip might be achieved by either
 245 narrowing the gap between the hot and cold arms or by reducing
 246 the width of the hot arm still further.

247 B. Frequency Dependence of Displacement

248 Square pulses with $t_{\text{on}} = t_{\text{off}}$ were used for experiments
 249 on the device dependence on frequency which was found to
 250 significantly influence the magnitude of the actuation that could
 251 be achieved. Fig. 5 shows the variation of the displacement,
 252 normalized by its maximum value, as a function of the driving
 253 frequency. As the frequency was increased from 1 Hz to values
 254 of ca. 50–100 Hz, the maximum observed displacement re-
 255 maind unchanged. However, with further increase in fre-
 256 quency, the tip displacement diminished, reducing gradually to
 257 zero when the frequency was on the order of 300–700 Hz.

258 The cooling processes of a U-shaped actuator of this scale
 259 will have time constants of between 1 and 10 ms [24], which
 260 are much greater than those associated with the Joule-heating
 261 process. Consequently, as the driving frequency is increased,
 262 cooling of the microactuator is suppressed, and the device will
 263 remain at an elevated temperature; hence, it is difficult for the
 264 actuator to deliver a significant displacement because of the
 265 small temperature difference between its hot and cold regions.
 266 The cutoff frequency of such a thermal actuator, defined as
 267 that frequency at which the effective displacement falls to zero,
 268 is thus determined mainly by the cooling process, which is a
 269 function of device dimensions and material properties [24]. For
 270 the devices used in these tests, the thermal cooling time constant
 271 based on the thermal conduction model through the bonding
 272 pads could be estimated, for example, using [24, eq. (9)],
 273 to be ca. 4 ms. This is comparable to those reported in [24]
 274 but rather more than those estimates of 0.5–0.2 ms made from
 275 the observed cutoff frequencies of several hundred Hertz. This
 276 difference might be attributable to an underestimation of heat

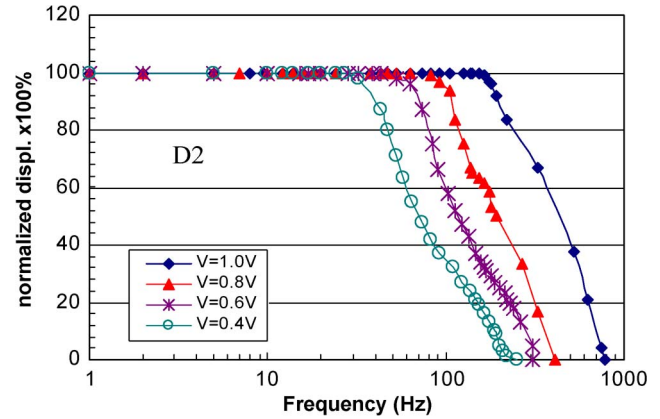


Fig. 6. Dependence of displacement on the frequency with peak voltage as a variable for device D2. It demonstrates that the cutoff frequency increases with increasing the voltage amplitude of the pulsed signal.

loss through other mechanisms such as conduction or radiation
 through the air [25], [26].

The frequency dependence of the displacement is also sig-
 nificantly affected by the amplitude of the pulse voltage. Fig. 6
 shows the dependence of the normalized displacement on fre-
 quency with voltage of the pulse as a variable. The cutoff
 frequency, as defined before, increases with the signal voltage.
 The reason for this behavior is not clear. The cooling process
 normally has an exponential relationship with time, i.e., cooling
 is faster at a high temperature. A higher temperature can
 be caused by a higher voltage pulse. Thus, a device with a
 high voltage pulse has a high cutoff frequency. The maximum
 temperature decreases when reducing the pulse voltage; thus,
 the cooling process becomes longer, and the cutoff frequency
 becomes smaller. Since the pulsewidth is much shorter than
 the 0.1 s used for the displacement measurements, the heating
 is not significant. However, a detailed observation revealed a
 back bending of up to $2 \mu\text{m}$ after the measurement at a signal
 voltage of 1.0V, indicating an average temperature rise of up
 to $\sim 200 \text{ }^\circ\text{C}$, although this is much smaller than $T_a \sim 450 \text{ }^\circ\text{C}$,
 measured for the 0.1-s pulse measurement. The results imply
 that caution is needed in explaining the frequency dependence
 of microactuators.

C. Back Bending and Plastic Deformation

Fig. 7(a) and (b) shows the optical images of a thermal
 microactuator before and after applying a pulse current of
 54 mA. It is apparent that the tip of the microactuator has
 become displaced from its original position by $\sim 15 \mu\text{m}$ in a
 direction opposite to that of the forward displacement, which is
 an example of the so-called back bending. Further increase in
 the current leads to blowup or burn-off near the middle of the
 hot arm, as shown in Fig. 7(c).

Figs. 2–4 also show the extent of back bending as a func-
 tion of applied current, power, and average temperature for
 the two devices tested. Initially, there is no back bending,
 and then, the magnitude of the back-bending displacement in-
 creases with average temperature and falls away as the average
 temperature increases above $450 \text{ }^\circ\text{C}$. Back bending occurs at
 an average temperature as low as $\sim 160 \text{ }^\circ\text{C}$ and reaches a

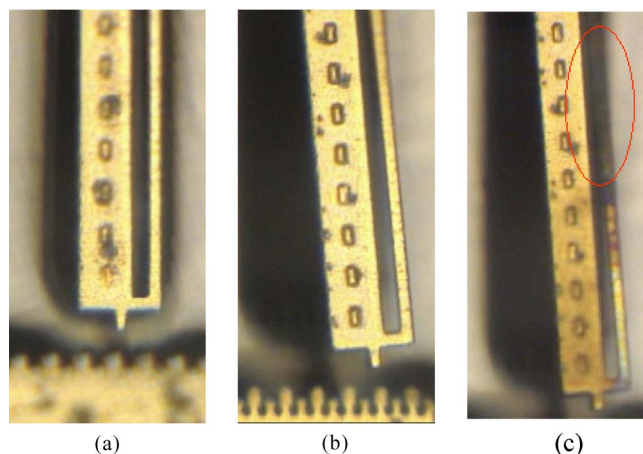


Fig. 7. Optical images of a thermal actuator show (a) the initial tip position and (b) the back bending after applying a pulse current of 54 mA and (c) burn-off followed by a high current of ~ 62 mA.

316 maximum backward displacement of $15 \mu\text{m}$ at $\sim 450^\circ\text{C}$, which
 317 is $\sim 75\%$ of the total forward displacement. The observed back-
 318 bending behavior with temperature for the D1 and D2 nickel
 319 microactuators is significantly different from that reported for
 320 silicon microactuators [6]. First, the average temperature of
 321 $\sim 160^\circ\text{C}$, which induces a measurable back bending for the
 322 nickel microactuators, is much lower than that of $\sim 660^\circ\text{C}$
 323 for the Si-based thermal actuators [6]. Second, while the back-
 324 bending displacement of the silicon actuators increases with
 325 power initially, it then remains at the maximum value as the
 326 power is further increased until the hot arm blows up [6]. Sil-
 327 icon is a relatively brittle material with a high melting tempera-
 328 ture, which can easily fracture or cleave along grain boundaries
 329 rather than softening at large stresses and high temperature.
 330 Further increases in temperature have been observed to lead
 331 to significant recrystallization and abnormal grain growth for
 332 polysilicon-based thermal actuators [10], [11]. Polysilicon re-
 333 crystallization to form large grain structures with crystal facets
 334 was observed at a temperature of 1100°C , which, while much
 335 lower than the melting temperature, roughly coincides with
 336 the temperature at which significant creep might be expected
 337 [9], [10]. Under a tensile stress at a high temperature, silicon
 338 plastic deformation is characterized by grain boundary separa-
 339 tion, internal cracking, and the formation of cavities [6], [10],
 340 rather than ductile necking.

341 Although nickel has a comparable melting temperature to
 342 silicon, it is ductile. The temperature to initiate plastic defor-
 343 mation in the nickel-based thermal actuators is much lower than
 344 that of comparable silicon microactuators. Since the estimated
 345 maximum temperature of the beam is $\sim 680^\circ\text{C}$, deformation
 346 by creep would seem to be responsible for the significant
 347 back-bending behavior of the nickel beams. Creep is thermally
 348 activated, so that both stress and temperature have profound
 349 effects on the process. Creep in metals can occur even at room
 350 temperature, provided that the stress level is sufficiently high
 351 [27]–[29]. This is significantly different from that of the silicon
 352 thermal actuators. As maximum temperature rises, the stress
 353 required to introduce creep in a nickel thermal actuator is much
 354 lower than that of a silicon actuator. Metals become much

more reactive at high temperatures, and metallic surfaces will
 be oxidized quickly at relatively low temperatures. However,
 the oxidation of surface seems unlikely to be instrumental in
 reducing the length of the hot arm as the volume of the material
 normally increases after oxidation, and so is unlikely to be the
 cause of the back bending of the nickel device.

The temperatures shown in Fig. 4 are the averages extracted
 from the variation of the resistances of the nickel microactua-
 tors D2. The maximum temperature is near the middle of the
 hot arm. A previous analysis based on the thermal conduction
 model indicated that the maximum temperature increase of the
 hot arm ΔT_{max} would be expected to be about 1.5 times the cal-
 culated average temperature increase ΔT_{ave} [21], [22]. Assum-
 ing an ambient temperature of 20°C , the average temperature of
 160°C shown in Fig. 7(b) corresponds to a maximum tempera-
 ture of $\sim 1.5 \times (160 - 20) + 20 = 230^\circ\text{C}$, i.e., close to 220°C
 suggested by Lee *et al.* [15]. The estimated average temperature
 of 450°C for severe degradation corresponds to a maximum
 temperature of $\sim 665^\circ\text{C}$, which should be high enough to
 induce significant creep, particularly at a large compressive
 stress. Furthermore, it is possible that these figures for average
 and maximum temperatures are underestimates as a result of
 the simplified model. The actual maximum temperature might
 exceed that estimated by $\sim 20\%$.

Device D1 showed smaller displacements in both forward
 displacement and back bending than those of the device D2,
 as shown in Figs. 2–4. It is believed to be caused by the thin Ni
 film, which is $3 \mu\text{m}$. When the film thickness is smaller than the
 width of the hot arm, a certain degree of out-of-plane buckling
 under thermal stress occurs. This will not introduce a plastic
 deformation, as it is well within the elastic state, but reduce the
 forward displacement and back bending.

In order to investigate the cause of back bending, the nickel
 microactuators were thermally stressed by passing a high cur-
 rent of 54 mA through the structure for 3 min, and the resulting
 changes in beam morphology were studied. The 54-mA current
 chosen for the experiment corresponds to the near-worst case
 of the back bending, as shown in Fig. 2. However, the average
 temperature was higher than that at 54 mA shown in Fig. 4, as
 the device was heated for 3 min, which is much longer than the
 0.1-s pulse measurement. The temperature increases, owing to
 the positive temperature coefficient of the resistivity. At the
 end of 3 min, the average temperature raised from $\sim 450^\circ\text{C}$ to
 $\sim 500^\circ\text{C}$, calculated from the increased resistance, correspond-
 ing to a maximum temperature of $\sim 1.5 \times (500 - 20) + 20 = 399$
 740°C . Fig. 8 shows the SEM images of a hot arm at various
 locations along its length after such a thermal treatment which
 illustrates some significant changes. Near the tip joint with the
 cold arm, the hot arm has retained the smooth surface finish
 of the original. At some distance from its ends, the surface of
 the hot arm becomes rougher and more rounded—evidence of
 plastic flow. Toward its mid-length, the beam cross section is
 significantly thinner, exhibiting a discernable neck. Near this
 position, on both sides of it, there is a significant accumulation
 or pileup of material. These changes in section, the general
 rounded appearance and lack of any preferred crystal facet,
 indicate that the metal has undergone a reflow process. As the
 melting temperature of nickel is 1455°C , it is unlikely that

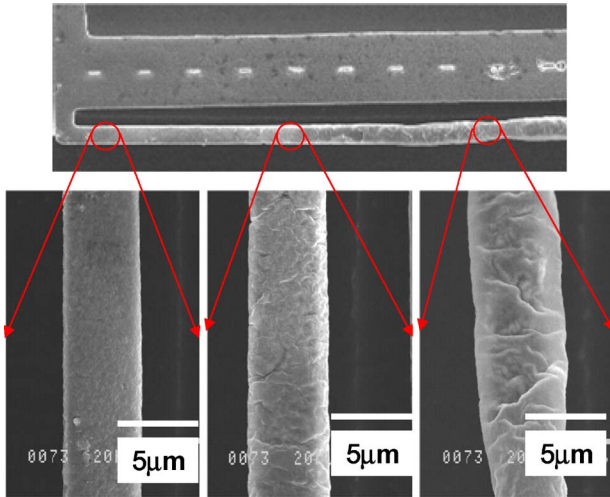


Fig. 8. SEM photographs of the hot arm in different places. The device had undergone heating by a current of 55 mA for 3 min. It showed the Ni pileup near the hotter places and necking at the hottest spot.

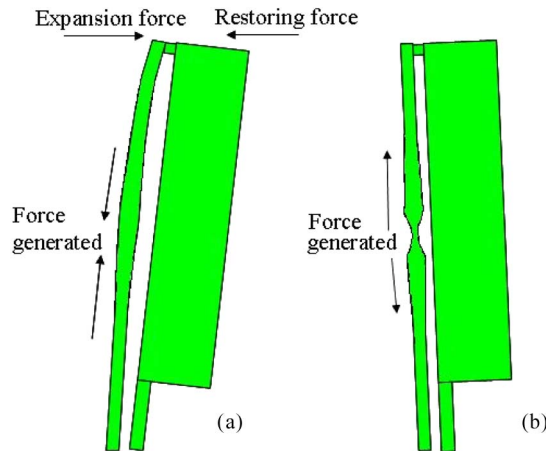


Fig. 9. (a) Schematic drawing of force acting on the hot arm when the current is applied; restoring force produces a compressive stress, leading to pileup of Ni. (b) When the current is removed, restoring force produces a tensile stress, leading to necking of the hot arm.

the reflow is caused by melting. It is believed that the material pileup and reflow are associated with creep encouraged by elevated temperatures and high stresses.

A dynamic model can thus be proposed for the plastic deformation of the nickel thermal microactuator shown schematically in Fig. 9. When the current is first applied, the differential Joule heating of the thinner arm causes it to become hotter, and thus, in an attempt to thermally lengthen by a greater margin than the adjacent cold arm, this puts the material under a compressive load. This compressive stress causes the material to deform and pile up in compression, the raised temperature accelerating this process. Nickel accumulates near the hottest section forming the comparatively large folded structures visible at this section of the beam. It is this effective shortening of the hot arm that is responsible for the subsequent back bending of the actuator. Upon removing the current, the beam rotates about its base as the force in the thinner arm changes from compressive stress to tensile stress. This tensile stress tends to elongate the shortened arm. Since the middle hottest section is

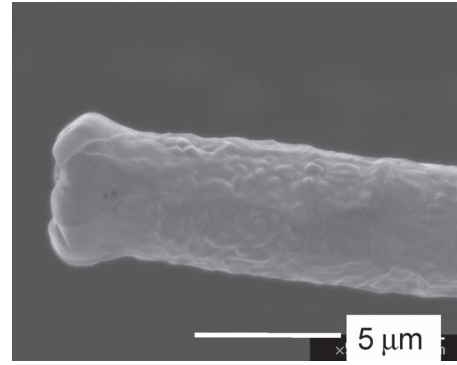


Fig. 10. SEM photograph of a blowup tip, showing a rounded structure which was caused by thermal runaway and melting.

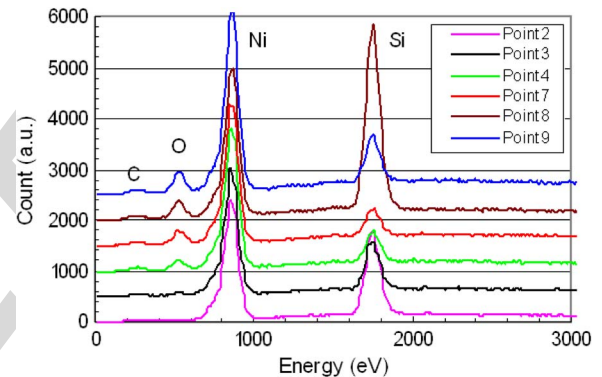


Fig. 11. EDX spectra from the surface of a hot arm after thermal stress at 55 mA for 3 min. As approaching the middle of the arm, the oxygen signal becomes much stronger.

the mechanically weakest, it is here that the extension occurs, manifesting itself as the observed neck.

It is thus the combination of pileup and necking that is believed to be responsible for the decreases in forward and back-bending displacements at $T_{ave} = T_0 + \Delta T_{ave} \Rightarrow 450^\circ\text{C}$, as shown in Fig. 4. At a modest temperature, material pileup leads to the shortening of the arm, causing the back bending and reduction of forward displacement upon removing the current. At $T_{ave} \Rightarrow 450^\circ\text{C}$, necking prevents further shortening of the arm; hence, the back-bending displacement decreases as the temperature increases further. Any further increase in the current increases the temperature rapidly principally because of the positive temperature coefficient of the resistivity of nickel, rapidly leading to blowup of the hot arm. Fig. 10 shows a SEM image of the tip of a failed arm, clearly showing the rounded reflow structure.

D. Thermal Oxidation of the Beam

The surface of the nickel beams can be easily oxidized in air at high temperatures, and this may significantly affect the performance of these thermal actuators as a result of gradual changes in their resistance and mechanical properties. EDX was used to characterize the element concentration along the hot arm of the device shown in Fig. 8, and the results are shown in Fig. 11. Point 2 corresponds to a position where the hot and cold arms are linked, and point 9 is close to the neck; intermediate

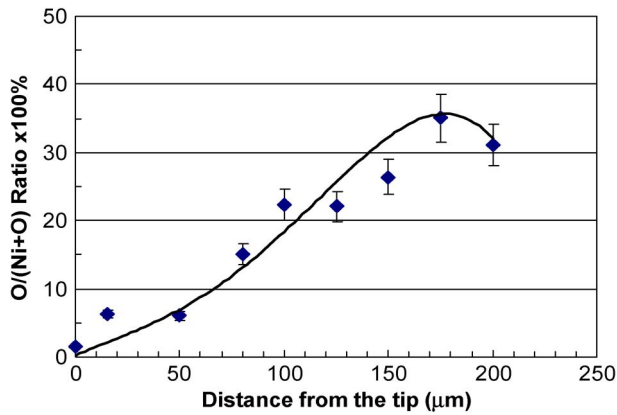


Fig. 12. Distribution of oxygen to Ni ratio along the hot arm. The oxygen content reaches the highest level at the middle of the hot arm.

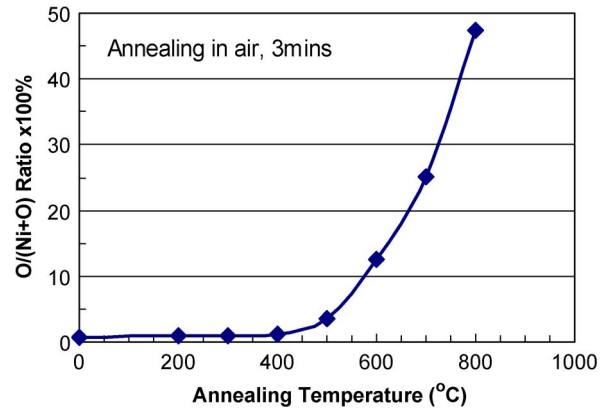


Fig. 13. Oxygen to nitrogen ratio as a function of annealing temperature for a Ni metal annealed in air for 3 min. The oxygen concentration increases rapidly as the temperature is over 450 °C and reaches ~36% at ~750 °C.

457 points are close to being equally spaced between them. The Si 458 signal is from the silicon substrate, as the scanning area of the 459 EDX measurements is wider than the hot arm width. Nickel 460 is the dominant peak with a small trace of carbon, which is 461 probably the residue from photoresist and plasma etching gases, 462 as well as some carbon absorbance from the ambient. The 463 oxygen concentration on the surface of the wide arm is typically 464 at the level of < 2% (near the detection limitation) and is 465 attributed to the thin native oxide and oxygen absorbance from 466 the ambient. Fig. 12 shows the oxygen concentration results 467 along the hot arm after the thermal overload treatment. The 468 oxygen concentration increases steadily from the arm edge and 469 reaches its highest value of ca. 36% roughly at the middle of the 470 hot arm. This clearly indicates that most of the hot arm surface 471 is oxidized after treatment with a 54-mA current maintained 472 for 3 min. The profile of the oxygen concentration along the 473 hot arm is also similar to the temperature profile obtained by 474 finite-element-analysis-based modeling [3], [25], implying that 475 the high temperature is directly responsible for the observed 476 oxidation.

477 For comparison, a series of electroplated Ni samples was also 478 annealed at temperatures from 200 °C to 800 °C for 3 min 479 in an air furnace (rapid thermal annealing), and their oxygen 480 concentration similarly investigated by EDX. The results are 481 shown in Fig. 13 as a function of the annealing temperature. 482 Up to 400 °C, the oxygen concentration remains below the 483 detection limitation but grows rapidly as the temperature in- 484 creases above 400 °C. The comparison of O/(O + Ni) ratios 485 along the hot arm of the actuator with those of the annealed 486 samples implies that the highest temperature of the hot arm was 487 around ~760 °C, which is in good agreement with the estimated 488 maximum temperature of 740 °C from the thermal conduction 489 model discussed before.

490 We also observed that the electrical resistance of the actuator 491 could be changed by the application of a current-driven thermal 492 cycle. This is illustrated by the data of Fig. 14 which shows 493 how the resistance of the device, measured at room temperature, 494 was influenced by the calculated average temperature during the 495 imposed thermal cycle. The resistance was measured at room 496 temperature by allowing the actuator to cool down prior to each 497 measurement, while the average temperature was calculated

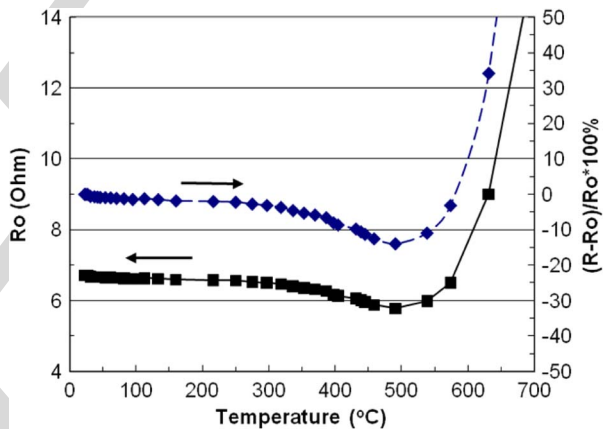


Fig. 14. Resistance of the thermal actuator as a function of average temperature measured. The resistance initially decreases, owing to annealing, and then increases rapidly when temperature exceeds 500 °C due to surface oxidation.

using the resistance measured when the current was on. As the 498 current increases, the average temperature rises. The resistance 499 of the device, determined principally by that of the hot arm, 500 initially slowly decreased with increasing temperatures up to 501 a value of ca. 500 °C, above which the resistance increased 502 rapidly, leading to thermal runaway and blowup. The initial 503 fall of the resistance with increasing average temperature is 504 believed to be caused by an annealing effect. Upon anneal- 505 ing at a modest temperature, an electroplated nickel structure 506 normally becomes dense with an increase in grain size and a 507 fall in resistance [30], [31]. Any further increase in average 508 temperature leads to severe surface oxidation, thus increasing 509 the resistance until the current path fails. The observed onset 510 temperature of ~500 °C for the resistance to increase rapidly 511 coincides with that of O/(Ni + O) ratio versus temperature pro- 512 file shown in Fig. 13. It is also clear that the resistance increases 513 dramatically after $T_{ave} \geq 500$ °C and reaches more than 150% 514 of its ambient value at 700 °C, at which the actuators become 515 sufficiently degraded to lead to a decreased displacement. It 516 can be concluded that both creep and the surface oxidation 517 at raised temperatures are responsible for the degradation in 518 displacement of the nickel thermal actuators.

520

IV. SUMMARY

521 U-shaped thermal microactuators were fabricated by a
522 single-mask process using electroplated nickel as the active
523 material. Their displacement and back bending have been char-
524 acterized, and their thermal degradation has been investigated
525 in detail. The results can be summarized as follows.

- 526 1) The nickel thermal actuators investigated delivered dis-
527 placements of up to 20 μm at an average temperature
528 of 450 $^{\circ}\text{C}$, which is much lower than those generally
529 required by Si-based microactuators. The displacement
530 strongly depends on the voltage amplitude of the pulse
531 signal used. The typical cutoff frequency for the thermal
532 actuators with a length of 400 μm was between 300 and
533 1000 Hz.
- 534 2) The phenomenon of back bending has been observed in
535 the chosen nickel-based thermal microactuators becom-
536 ing evident at average temperatures as low as 160 $^{\circ}\text{C}$: This
537 corresponds to a maximum temperature of 240 $^{\circ}\text{C}$ in the
538 hot beam. These values are much lower than what would
539 be expected in the case of silicon-based microactuators.
- 540 3) The magnitudes of both forward and back-bending dis-
541 placements have become larger with increases in tem-
542 perature up to 450 $^{\circ}\text{C}$, but then have been subsequently
543 decreased with temperature. Plastic deformation at high
544 temperature and surface oxidation of the nickel hot arm
545 are responsible for this phenomenon.
- 546 4) Reflow of the nickel has occurred under a compressive
547 stress at raised temperatures, which can cause the material
548 to pile up and thus make the beam locally larger in
549 cross section. Conversely, a tensile stress generated upon
550 the removal of the current can cause necking and local
551 thinning of the hot arm.
- 552 5) EDX characterization has revealed that the surface of
553 the hot arm is almost fully oxidized at a temperature
554 of ~ 750 $^{\circ}\text{C}$, leading to a rapid increase of the resistance
555 of the overall device.
- 556 6) Both plastic deformation and surface oxidation at raised
557 temperatures have been responsible for the reduction in
558 the available displacement of thermal actuators.

559

REFERENCES

560 [1] J. R. Reid, V. M. Bright, and J. H. Comtois, "Force measurements of
561 polysilicon thermal micro-actuators," *Proc. SPIE*, vol. 2882, pp. 296–306,
562 1996.

563 [2] T. Moulton and G. K. Ananthasuresh, "Micromechanical devices with
564 embedded electro-thermal-compliant actuation," *Sens. Actuators A, Phys.*,
565 vol. 90, no. 1/2, pp. 38–48, May 2001.

566 [3] Q. A. Huang and N. K. Lee, "Analysis and design of polysilicon thermal
567 flexure actuator," *J. Micromech. Microeng.*, vol. 9, no. 1, pp. 64–70,
568 Mar. 1999.

569 [4] R. L. Borwick, P. A. Stupar, and J. DeNatale, "A hybrid approach to low-
570 voltage MEMS switches," in *Proc. 12th Int. Conf. Transducer, Solid-State*
571 *Sens., Actuators Microsyst.*, 2003, vol. 1, pp. 859–862.

572 [5] J. H. Comtois and V. M. Bright, "Applications for surface-micromachined
573 polysilicon thermal actuators and arrays," *Sens. Actuators A, Phys.*,
574 vol. 58, no. 1, pp. 19–25, Jan. 1997.

575 [6] S. Deladi, G. Krijnen, and M. Elwenspoek, "Distinction of the irreversible
576 and reversible actuation regions of B-doped poly-Si based electrother-
577 mal actuators," *J. Micromech. Microeng.*, vol. 14, no. 9, pp. S31–S36,
578 Sep. 2004.

[7] J. Bagdahn and W. N. Sharp, "Fracture strength of polysilicon at stress 579
concentration," *J. Microelectromech. Syst.*, vol. 12, no. 3, pp. 302–312, 580
Jun. 2003.

[8] J. M. Maloney, D. S. Schreiber, and D. L. DeVoe, "Large-force elec- 582
trothermal liner micromotors," *J. Micromech. Microeng.*, vol. 14, no. 2, 583
pp. 226–234, Feb. 2004.

[9] R. A. Conant and R. S. Muller, "Cyclic fatigue testing of surface- 585
micromachined thermal actuators," in *Proc. ASME*, 1998, vol. DSC-V.66, 586
pp. 273–277.

[10] S. Nakao, T. Ando, M. Shikeda, and K. Sato, "Mechanical proper- 588
ties of a micron-sized SCS film in a high-temperature environment," *J.* 589
Micromech. Microeng., vol. 16, no. 4, pp. 715–720, Apr. 2006.

[11] A. Tuck, A. Jungen, A. Geisberger, M. Ellis, and G. Skidmore, "A study 591
of creep in polysilicon MEMS devices," *J. Eng. Mater. Technol.*, vol. 127, 592
no. 1, pp. 90–96, Jan. 2005.

[12] J. K. Luo, J. H. He, A. J. Flewitt, D. F. Moore, S. M. Spearing, N. A. Fleck, 594
and W. I. Milne, "Development of all metal electro-thermal actuators 595
and its applications," *J. Microlith. Microfab. Microsyst.*, vol. 4, no. 2, 596
p. 023 012-1, 2005.

[13] P. M. Zavracky, S. Majumder, and N. E. McGruer, "Micromechanical 598
switches fabricated using nickel surface micromachining," *J. Micro-* 599
electromech. Syst., vol. 6, no. 1, pp. 3–9, Mar. 1997.

[14] I. Schiele, J. Huber, B. Hillerich, and F. Kozlowski, "Surface- 601
micromachined electrostatic microrelay," *Sens. Actuators A, Phys.*, 602
vol. 66, no. 1–3, pp. 345–354, Apr. 1998.

[15] J. S. Lee, S. D. Park, A. K. Nallani, G. S. Lee, and J. B. Lee, "Sub-micron 604
metallic electrothermal actuators," *J. Micromech. Microeng.*, vol. 15, 605
no. 2, pp. 322–327, Feb. 2005.

[16] D. A. Fanner and R. A. F. Hammond, "The properties of nickel 607
electrodeposited from a sulphamate bath," *Trans. Inst. Met. Finish.*, 608
vol. 36, pp. 32–42, 1959.

[17] L. S. Stephens, K. W. Kelly, S. Simhadri, A. B. McCandless, and 610
E. I. Meletis, "Mechanical property evaluation and failure analysis of 611
cantilevered LIGA nickel microposts," *J. Microelectromech. Syst.*, vol. 10, 612
no. 3, pp. 347–359, Sep. 2001.

[18] F. Wang, R. Cheng, and X. Li, "MEMS vertical probe cards with ultra 614
densely arrayed metal probes for wafer-level IC testing," *J. Microelectro-* 615
mech. Syst., vol. 18, no. 4, pp. 933–941, Aug. 2009.

[19] R. V. Shenoy and M. Datta, "Effect of mask wall angle on shape evolution 617
during through-mask electrochemical micromachining," *J. Electrochem.* 618
Soc., vol. 143, no. 2, pp. 544–552, 1996.

[20] J. K. Luo, D. P. Chu, A. J. Flewitt, S. M. Spearing, N. A. Fleck, and 620
W. I. Milne, "Uniformity control of Ni thin film microstructure deposited 621
by through-mask plating," *J. Electrochem. Soc.*, vol. 152, no. 1, pp. C36– 622
C41, 2005.

[21] J. K. Luo, A. J. Flewitt, S. M. Spearing, N. A. Fleck, and W. I. Milne, 624
"Comparison of microtweezers based on three lateral thermal actuator 625
configurations," *J. Micromech. Microeng.*, vol. 15, no. 6, pp. 1294–1302, 626
Jun. 2005.

[22] J. K. Luo, A. J. Flewitt, S. M. Spearing, N. A. Fleck, and W. I. Milne, 628
"Three types of planar structure microspring electro-thermal actuators 629
with insulating beam constraint," *J. Micromech. Microeng.*, vol. 15, no. 8, 630
pp. 1527–1535, Aug. 2005.

[23] J. K. Luo, M. Pritschow, A. J. Flewitt, S. M. Spearing, N. A. Fleck, and 632
W. I. Milne, "Effects of process conditions on properties of electro- 633
plated Ni thin films for microsystems applications," *J. Electrochem. Soc.*, 634
vol. 153, no. 10, pp. D155–D161, 2005.

[24] E. T. Enikov and K. Lazarov, "PCB-integrated metallic thermal micro- 636
actuators," *Sens. Actuators A, Phys.*, vol. 105, no. 1, pp. 76–82, Jun. 2003. 637

[25] R. Hickey, D. Sameoto, T. Hubbard, and M. Kujath, "Time and frequency 638
response of two-arm micromachined thermal actuators," *J. Micromech.* 639
Microeng., vol. 13, no. 1, pp. 40–46, Jan. 2003.

[26] R. Kickey, M. Kujath, and T. Hubbard, "Heat transfer analysis and opti- 641
mization of two-beam microelectromechanical thermal actuators," *J. Vac.* 642
Sci. Technol. A, Vac. Surf. Films, vol. 20, no. 3, pp. 971–974, May 2002. 643

[27] Z. Budrovic, H. V. Swygenhoven, P. M. Derlet, S. V. Petegem, and 644
B. Schmitt, "Plastic deformation with reversible peak broadening in 645
nanocrystalline nickel," *Science*, vol. 304, no. 5668, pp. 273–276, 646
Apr. 2004.

[28] X. Z. Liao, A. R. Kilmametov, R. Z. Valiev, H. Gao, X. Li, 648
A. K. Mukherjee, J. F. Binger, and Y. T. Zhu, "High-pressure torsion- 649
induced grain growth in electrodeposited nanocrystalline Ni," *Appl. Phys.* 650
Let., vol. 88, no. 21, p. 021 909, May 2006.

[29] G. J. Fan, Y. D. Wang, L. F. Fu, H. Choo, P. K. Liaw, Y. Ren, and 652
W. N. D. Browning, "Orientation-dependent grain growth in a bulk nanocryst- 653
alline alloy during the uniaxial compressive deformation," *Appl. Phys.* 654
Let., vol. 88, no. 17, p. 171 914, Apr. 2006. 655

656 [30] S. C. Chang, J. M. Shieh, B. T. Dai, M. S. Feng, and Y. H. Li, "The effect
657 of plating current density on self-annealing behaviours of electroplated
658 copper film," *J. Electrochem. Soc.*, vol. 149, no. 9, pp. G535–G538, 2002.
659 [31] W. H. Safranek, "Structure and property relationship for bulk electrode-
660 posits," *J. Vac. Sci. Technol.*, vol. 11, no. 4, pp. 765–770, 1974.

Y. Q. Fu, photograph and biography not available at the time of publication. 662 **AQ5**

J. A. Williams, photograph and biography not available at the time of 663 **AQ6**
publication. 664

AQ4 661 **J. K. Luo**, photograph and biography not available at the time of publication.

W. I. Milne, photograph and biography not available at the time of publication. 665 **AQ7**

IEEE
Proof

AUTHOR QUERIES

AUTHOR PLEASE ANSWER ALL QUERIES

AQ1 = The acronym “EPSRC” was defined as “Engineering and Physical Sciences Research Council.”
Please check if correct.

AQ2 = The acronym “MEMS” was defined as “microelectromechanical system.” Please check if correct.

AQ3 = Please provide complete title of proceedings in Ref. [9].

AQ4 = Please provide photograph and biography of author J. K. Luo.

AQ5 = Please provide photograph and biography of author Y. Q. Fu.

AQ6 = Please provide photograph and biography of author J. A. Williams.

AQ7 = Please provide photograph and biography of author W. I. Milne.

END OF ALL QUERIES

IEEE
Proof

Thermal Degradation of Electroplated Nickel Thermal Microactuators

J. K. Luo, Y. Q. Fu, J. A. Williams, and W. I. Milne

Abstract—In this paper, the thermal degradation of laterally operating thermal actuators made from electroplated nickel has been studied. The actuators investigated delivered a maximum displacement of ca. 20 μm at an average temperature of $\sim 450^\circ\text{C}$, which is much lower than that of typical silicon-based microactuators. However, the magnitude of the displacement strongly depended on the frequency and voltage amplitude of the pulse signal applied. Back bending was observed at maximum temperatures as low as 240°C . Both forward and backward displacements grew as the applied power was increased up to a value of 60 mW; further increases led to reductions in the magnitudes of both displacements. Scanning electron microscopy clearly showed that the nickel beams began to deform and change their shape at this critical power level. Compressive stress is responsible for nickel pileup, while tensile stresses, generated upon removing the current, are responsible for necking at the hottest section of the hot arm of the device. Energy dispersive X-ray diffraction analysis also revealed the severe oxidation of Ni structure induced by Joule heating. The combination of plastic deformation and oxidation was responsible for the observed thermal degradation. Results indicate that nickel thermal microactuators should be operated below 200°C to avoid thermal degradation. [2009-0015]

Index Terms—Back bending, electroplating, oxidation, plastic deformation, thermal actuator, thermal degradation.

I. INTRODUCTION

THE ATTRACTION of microelectrothermal actuators for use in microsystems and microelectronics lies in the relatively large forces and displacements which they can generate [1]–[3]. With operational voltages comparable to those used in CMOS, they are particularly suitable for integration with electronic circuits for control and signal processing. In general, microactuators have longer lifetimes than their macro counterparts, owing to the reduced number of defects in components with such small linear dimensions. The operational durability and reliability of microactuators are thus generally superior

Manuscript received January 15, 2009; revised September 15, 2009. The work of J. K. Luo was supported in part by the Engineering and Physical Sciences Research Council under Project EP/D051266. Subject Editor M. Wong.

J. K. Luo is with the Engineering Department, University of Cambridge, Cambridge, CB3 0FA, U.K., and also with the Centre for Material Research and Innovation, University of Bolton, Bolton, BL3 5AB, U.K. (e-mail: j2.bolton.ac.uk.).

Y. Q. Fu is with the Engineering Department, University of Cambridge, Cambridge, CB3 0FA, U.K., and also with the Department of Mechanical Engineering, School of Engineering and Physical Sciences, Heriot Watt University, Edinburgh, EH14 4AS, U.K.

J. A. Williams and W. I. Milne are with the Engineering Department, University of Cambridge, Cambridge, CB3 0FA, U.K.

Color versions of one or more of the figures in this paper are available online at <http://ieeexplore.ieee.org>.

Digital Object Identifier 10.1109/JMEMS.2009.2034394

to macroactuators. Microelectromechanical system (MEMS) switches and comb-drive structures based on electrostatic actuation have been operated up to tens of billion of cycles without failure [4]. However, thermal microactuators have shorter lifetimes, particularly when operated at high temperatures. When operated in these conditions, deterioration in actuation force and actuation frequency, as well as degradation in maximum displacement and catastrophic failure by burn-off or blowup, has been reported for both lateral and vertical thermal microactuators [5], [6]. Thermal degradation is attributable to both surface oxidation and plastic deformation caused by material creep at elevated temperatures. When a thermal microactuator is heated above some critical temperature, it may undergo localized material deformation, oxidation, creep, or even recrystallization in the most vulnerable position [5], [6]. In Si-based actuators, a structural deformation phenomenon, known as “back bending,” is often observed, whereby the actuating elements will not return to their original positions once they have been “overactuated” but are left permanently bent or deformed in the direction opposite to that of normal actuation.

Plastic deformation caused by creep and recrystallization increases rapidly with temperature. For a typical lateral thermal actuator consisting of a combination of hot and cold arms, as shown in Fig. 1(a), the highest temperature occurs near the middle of the hot arm; however, the largest stress usually occurs either near the joint of the hot and cold arms or at the root of the beams or flexures which allow the structure to move. If material creep exists at a raised temperature, we should expect material pileup or accumulation to occur at the place where the compressive stress is the largest. Although there is no direct reported evidence of such compressive deformation, tensile tests of Si microbeams, at various elevated temperatures, have revealed thinning due to creep [7]. The temperature required for plastic deformation in a Si actuator is believed to be correlated with the intrinsic melting temperature ($\sim 1414^\circ\text{C}$) of this material [8]. The observed plastic deformation transition temperature for Si actuators, however, is typically $600^\circ\text{C} \sim 800^\circ\text{C}$ [6], which is much lower than the intrinsic melting temperature of silicon. It was believed that the plastic deformation of the silicon actuators is dominated by brittle-to-ductile transition temperature which is $\sim 660^\circ\text{C}$ [9], which is within the observed plastic deformation transition temperatures ($600^\circ\text{C} \sim 800^\circ\text{C}$) for silicon thermal actuators. Although thermal degradation has been studied in microactuators for many years [5]–[11], the degradation mechanisms are still not clear.

Silicon is the dominant material used for MEMS devices not least because of the suite of microfabrication technologies and

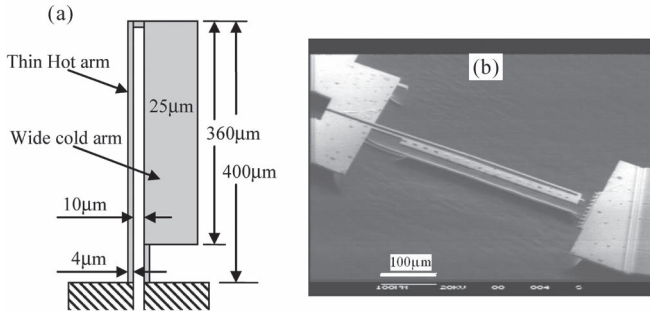


Fig. 1. (a) Schematic drawing of the U-shaped thermal microactuator. (b) SEM photograph of the U-shaped Ni thermal microactuator.

87 manufacturing facilities inherited from the microelectronics
88 industry. Since metals have higher thermal expansion coeffi-
89 cients than silicon, metallic thermal microactuators have lower
90 operation temperatures. For example, if a Si actuator needs an
91 operation temperature around 1000 °C to deliver a particular
92 displacement, then a Ni-based actuator would only require a
93 temperature of ~400 °C [12]. In addition, nickel-based actua-
94 tors have much lower resistivity and are thus particularly suit-
95 able for microactuator-based microrelays and microswitches
96 [13], [14].

97 Nickel and Ni-Fe alloys are the most studied metals for
98 microactuators because of their attractive material properties
99 and easy fabrication by electroplating [12], [13]. Although
100 nickel has a high melting temperature (1455 °C), which is
101 higher than that of silicon (1414 °C), it is ductile in nature.
102 Metals oxidize at much lower temperatures than silicon, and
103 thus, the temperature limitation of a metal device is expected to
104 be much lower than its silicon counterpart. Indeed, a limiting
105 temperature of ~200 °C has been suggested for the nickel ther-
106 mal actuators, although with little experimental support [15].
107 The degradation of electrodeposited Ni structures and devices
108 has been studied under high stress by many groups, [16]–[18]
109 but mostly at room temperatures. There is a lack of studies on
110 Ni microstructures and devices under thermal stress. This paper
111 reports a systematic investigation on the thermal degradation of
112 a nickel thermal microactuator, including back bending, creep,
113 and oxidation.

114 II. FABRICATION AND ELECTRICAL TESTING

115 Fig. 1(a) shows a schematic drawing of the U-shaped lateral
116 thermal actuators used for this investigation. Each device con-
117 sisted of a thin hot arm and a wider cold arm joined by a thin
118 flexure. All the U-shaped actuators used in this paper had the
119 same dimensions. The length and width of the hot arms were
120 400 and 4 μm, respectively, with the corresponding dimensions
121 of the cold arms being 360 and 25 μm. The flexure at the
122 base of the cold arm was 40 μm long and 4 μm wide, and
123 the gap between the hot and cold arms was 10 μm. When a
124 current passes through a resistive device, its temperature rises
125 through Joule heating. In the case of a thermoelectric actuator,
126 the higher electrical resistance of the thinner beam leads to its
127 reaching a much higher temperature than the cold arm. This, in
128 turn, generates a greater change in length by thermal expansion,

thus producing a deflection of the free tip laterally toward the
cold arm.

The microactuators used in this paper were made from elec-
troplated nickel films using a through-mask-plating technology
[19], [20]. The devices were fabricated using a single-mask
process on a 4-in Si wafer: The details of the process can be
found in [12] and [21]. The thicknesses of the nickel films
for two batches of devices, designated hereafter as D1 and
D2, were 3 and 4 μm, respectively. The devices were released
by etching the Si underneath the nickel beams using a SF₆
reactive ion etch process. The plasma etching conditions were
as follows: a SF₆ flow rate of 45 sccm, a pressure of 150 mtorr,
an RF power of 150 W, and an etch time of 15 min. The
etch duration was long enough to remove all residual silicon
from the back of the devices which were separated from the
Si substrate by an air gap of 25–30 μm, which is sufficient
to minimize conductive losses. Fig. 1(b) shows a scanning
electron microscopy (SEM) of the D2 nickel microactuator with
a Ni thickness of ~4 μm. The surfaces of the devices were
smooth with a typical roughness of less than 20 nm, and the
sidewalls were almost vertical.

Electrical tests were conducted on the actuators using a probe
station. The motion of the actuators was captured by a video
camera with a resolution of 0.5 μm and was subsequently
analyzed by a commercial software. The actuators were driven
by a pulsed current using a Keithley voltage source Type 224,
which simultaneously monitored the voltage drop across the
devices, so that the power consumption and resistance of the
actuator could be calculated. A rising temperature will increase
the electrical resistance of the device due to the positive tem-
perature coefficient of the resistivity of metals. The average
temperature change of the thermal microactuator ΔT_{ave} can be
extracted from the change of the resistance by the relation [22]

$$\Delta T_{ave} = T - T_0 = (R(T) - R_0) / R_0 \xi \quad (1)$$

where T_0 is the room temperature, R_0 and $R(T)$ are the re-
sistances of the device at room temperature and the raised tem-
perature, respectively, and ξ is the temperature coefficient of the
resistivity of the Ni with a value of $3 \times 10^{-3} \text{ K}^{-1}$ obtained from
our previous work [23]. A metal such as nickel can be easily
oxidized at high temperatures, so that the resistance of the actu-
ator will increase during high-temperature measurements. This
may cause an underestimation of the device temperature. Since
significant metal oxidation occurs at temperatures $> 450^\circ\text{C}$,
except for those specific experiments observing the enhanced
deformation and oxidation processes, pulsed low currents were
used for the measurements to keep the surface temperature of
the beams at levels at which oxidation would be minimal.

The off-power tip position of a microactuator may gradually
shift due to the so-called back-bending effect, and the resistance
may also change after each measurement. In order to deter-
mine an accurate tip forward displacement and a back-bending
displacement, it was necessary to measure both the off-power
tip position (i.e., the back bent position) and resistance be-
fore starting each measurement. The measurement procedures
were as follows: 1) Measure the off-power position and resis-
tance; 2) apply a pulse current; 3) measure the corresponding

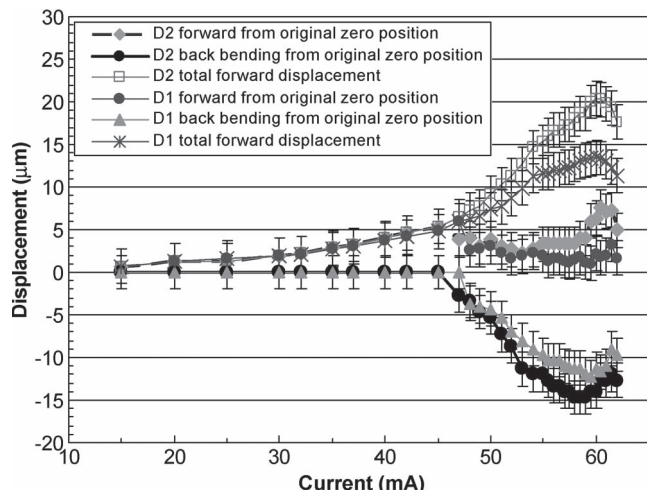


Fig. 2. Displacements of the Ni actuators as a function of pulsed current. The current pulsewidth was 0.1 s. Device D1 and D2 have different Ni thicknesses of 3 and 4 μm .

184 displacement and the voltage drop for resistance and power
 185 calculations; 4) turn off the current; and 5) remeasure the
 186 off-power position and resistance as part of the next measure-
 187 ment sequence. Metals have a positive temperature coefficient
 188 of resistivity, so that if the cooling of the hot arm is insufficient,
 189 then this element of positive feedback can lead to thermal run-
 190 away and structural failure. For the majority of the experiments,
 191 the current pulse duration was therefore limited to 0.1 s to
 192 avoid overheating and thermal destruction. However, in order
 193 to investigate the deformation and oxidation of the nickel beam
 194 that can occur in extreme circumstances, some experiments
 195 were carried out in which a current sufficient to generate the
 196 largest displacement of the actuator was applied to the actuator
 197 for a duration of 3 min. The subsequent surface morphology
 198 of the Ni beams was then characterized using field emission
 199 SEM (JEOL 6340F). Elemental concentrations at the surfaces
 200 of the nickel beams were measured using an energy dispersive
 201 X-ray (EDX) analyzer. The bonded oxygen content in the NiO_2
 202 formed during operation could be calculated from the intensity
 203 of the EDX curves.

III. RESULTS AND DISCUSSIONS

205 A. Displacement Versus Power

206 Two nickel thermal actuators D1 and D2 with nickel film
 207 thicknesses of 3 and 4 μm , respectively, were studied. Fig. 2
 208 shows the observed displacement from the original zero posi-
 209 tion, back bending, and the total forward displacement, which is
 210 the sum of the former two, with current as input variable. Fig. 3
 211 shows the back bending and the total forward displacement as
 212 a function of power calculated using the current applied and
 213 the resistance measured. The back-bending displacements were
 214 measured from the original zero position, and the minus sign
 215 represents its displacement opposite to the forward displace-
 216 ment. The total forward displacements (forward displacement
 217 in short hereinafter) of the thermal microactuator tips increased
 218 parabolically with the current applied and, up to an input of
 219 60 mW, were roughly proportional to the applied power, in

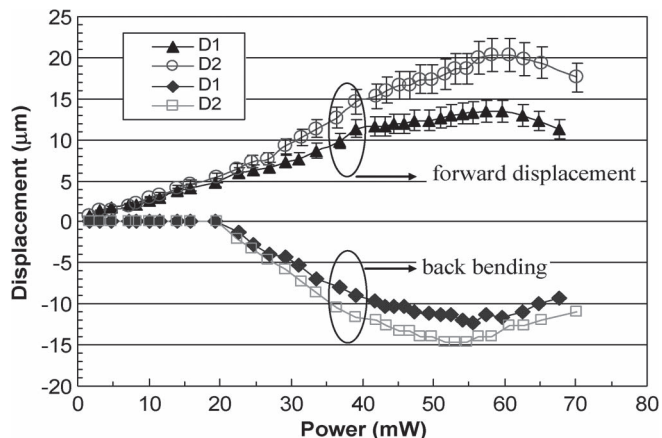


Fig. 3. Forward displacements and back bending of the Ni actuators as a function of power consumed, which were calculated from the current applied and voltage measured. The back bending appears at a current larger than 20 mA.

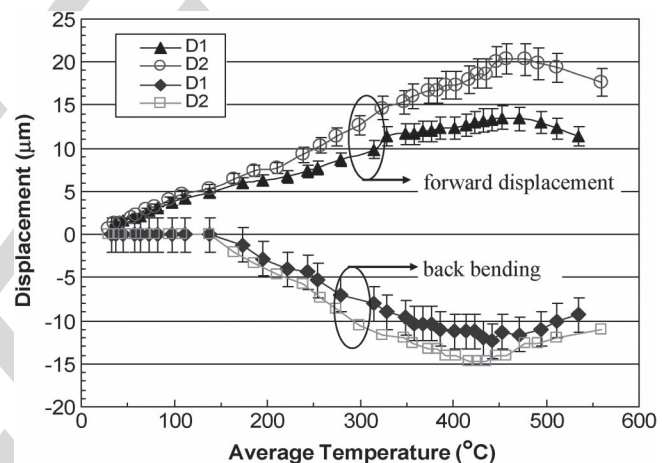


Fig. 4. Forward displacements and back bending as a function of average temperature extracted for two thermal actuators. The forward displacement is almost proportional to the average temperature. The back bending appears at an average temperature larger than 140 $^{\circ}\text{C}$.

220 agreement with theoretical analysis in the literature [12], [22].
 221 For both D1 and D2, the displacement of the tip reached a 221
 222 maximum at a power of 60 mW, specifically at values of 222
 223 ~ 16 and 20 μm , respectively; beyond this, the displacement 223
 224 decreased with any further increase in power due to thermal 224
 225 degradation, as discussed later. 225

226 The observed forward displacement and back bending of the 226
 227 microactuators D1 and D2 are shown in Fig. 4 as a function of 227
 228 their average temperatures calculated by (1). The displacement 228
 229 is approximately proportional to the average temperature up 229
 230 to a value of 450 $^{\circ}\text{C}$, above which the displacement decreases: 230
 231 This may well be due to thermal degradation, as discussed 231
 232 later. For a similar displacement, a Si-based thermal actuator 232
 233 would typically require an average temperature of over 1000 $^{\circ}\text{C}$ 233
 234 [4], [5]. The much lower operating temperatures of nickel 234
 235 actuators are attributable to their larger thermal expansion 235
 236 coefficient $\alpha = 15 \times 10^{-6} \text{ K}^{-1}$ compared to that of silicon for 236
 237 which $\alpha = 2.5 \times 10^{-6} \text{ K}^{-1}$. 237

238 The reported tip displacement for U-shaped actuators is 238
 239 typically $\sim 5\%$ of the length of the hot arm [5]. The observed 239

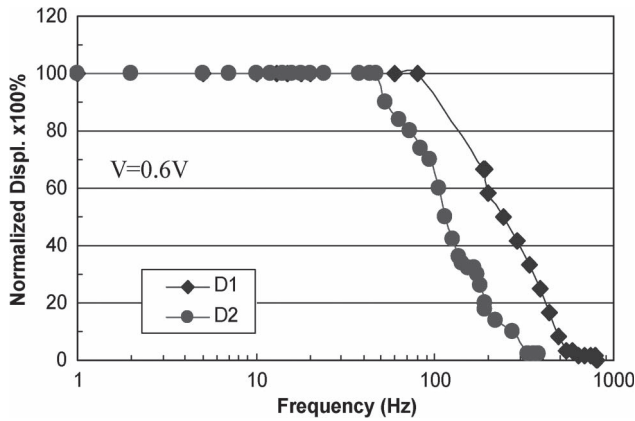


Fig. 5. Dependence of normalized displacements of Ni actuators on the frequency. The displacement remains unchanged at a frequency smaller than 40–100 Hz; it decreases with increasing the frequency and diminishes at a frequency higher than 300–700 Hz.

240 displacement of $\sim 20 \mu\text{m}$ for nickel devices with a length of
 241 $400 \mu\text{m}$ is therefore comparable to those reported for silicon
 242 actuators [1], [5] but occurs at a much low operating tempera-
 243 ture. Further reductions in the temperature required or increases
 244 in the displacements of the tip might be achieved by either
 245 narrowing the gap between the hot and cold arms or by reducing
 246 the width of the hot arm still further.

247 B. Frequency Dependence of Displacement

248 Square pulses with $t_{\text{on}} = t_{\text{off}}$ were used for experiments
 249 on the device dependence on frequency which was found to
 250 significantly influence the magnitude of the actuation that could
 251 be achieved. Fig. 5 shows the variation of the displacement,
 252 normalized by its maximum value, as a function of the driving
 253 frequency. As the frequency was increased from 1 Hz to values
 254 of ca. 50–100 Hz, the maximum observed displacement re-
 255 maind unchanged. However, with further increase in fre-
 256 quency, the tip displacement diminished, reducing gradually to
 257 zero when the frequency was on the order of 300–700 Hz.

258 The cooling processes of a U-shaped actuator of this scale
 259 will have time constants of between 1 and 10 ms [24], which
 260 are much greater than those associated with the Joule-heating
 261 process. Consequently, as the driving frequency is increased,
 262 cooling of the microactuator is suppressed, and the device will
 263 remain at an elevated temperature; hence, it is difficult for the
 264 actuator to deliver a significant displacement because of the
 265 small temperature difference between its hot and cold regions.
 266 The cutoff frequency of such a thermal actuator, defined as
 267 that frequency at which the effective displacement falls to zero,
 268 is thus determined mainly by the cooling process, which is a
 269 function of device dimensions and material properties [24]. For
 270 the devices used in these tests, the thermal cooling time constant
 271 based on the thermal conduction model through the bonding
 272 pads could be estimated, for example, using [24, eq. (9)],
 273 to be ca. 4 ms. This is comparable to those reported in [24]
 274 but rather more than those estimates of 0.5–0.2 ms made from
 275 the observed cutoff frequencies of several hundred Hertz. This
 276 difference might be attributable to an underestimation of heat

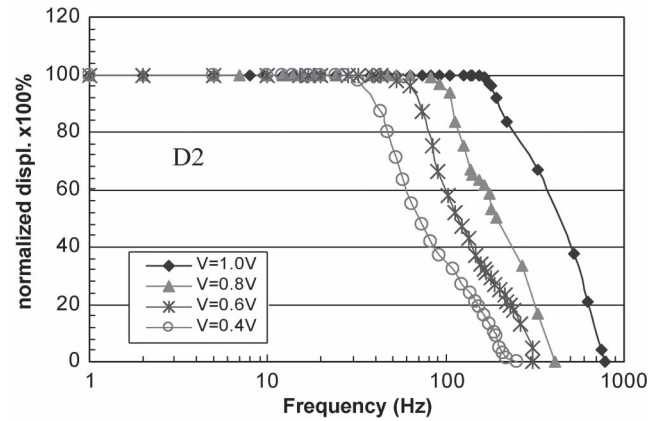


Fig. 6. Dependence of displacement on the frequency with peak voltage as a variable for device D2. It demonstrates that the cutoff frequency increases with increasing the voltage amplitude of the pulsed signal.

loss through other mechanisms such as conduction or radiation
 through the air [25], [26].

The frequency dependence of the displacement is also sig-
 nificantly affected by the amplitude of the pulse voltage. Fig. 6
 shows the dependence of the normalized displacement on fre-
 quency with voltage of the pulse as a variable. The cutoff
 frequency, as defined before, increases with the signal voltage.
 The reason for this behavior is not clear. The cooling process
 normally has an exponential relationship with time, i.e., cooling
 is faster at a high temperature. A higher temperature can
 be caused by a higher voltage pulse. Thus, a device with a
 high voltage pulse has a high cutoff frequency. The maximum
 temperature decreases when reducing the pulse voltage; thus,
 the cooling process becomes longer, and the cutoff frequency
 becomes smaller. Since the pulsewidth is much shorter than
 the 0.1 s used for the displacement measurements, the heating
 is not significant. However, a detailed observation revealed a
 back bending of up to $2 \mu\text{m}$ after the measurement at a signal
 voltage of 1.0V, indicating an average temperature rise of up
 to $\sim 200 \text{ }^\circ\text{C}$, although this is much smaller than $T_a \sim 450 \text{ }^\circ\text{C}$,
 measured for the 0.1-s pulse measurement. The results imply
 that caution is needed in explaining the frequency dependence
 of microactuators.

C. Back Bending and Plastic Deformation

Fig. 7(a) and (b) shows the optical images of a thermal
 microactuator before and after applying a pulse current of
 54 mA. It is apparent that the tip of the microactuator has
 become displaced from its original position by $\sim 15 \mu\text{m}$ in a
 direction opposite to that of the forward displacement, which is
 an example of the so-called back bending. Further increase in
 the current leads to blowup or burn-off near the middle of the
 hot arm, as shown in Fig. 7(c).

Figs. 2–4 also show the extent of back bending as a func-
 tion of applied current, power, and average temperature for
 the two devices tested. Initially, there is no back bending,
 and then, the magnitude of the back-bending displacement in-
 creases with average temperature and falls away as the average
 temperature increases above $450 \text{ }^\circ\text{C}$. Back bending occurs at
 an average temperature as low as $\sim 160 \text{ }^\circ\text{C}$ and reaches a

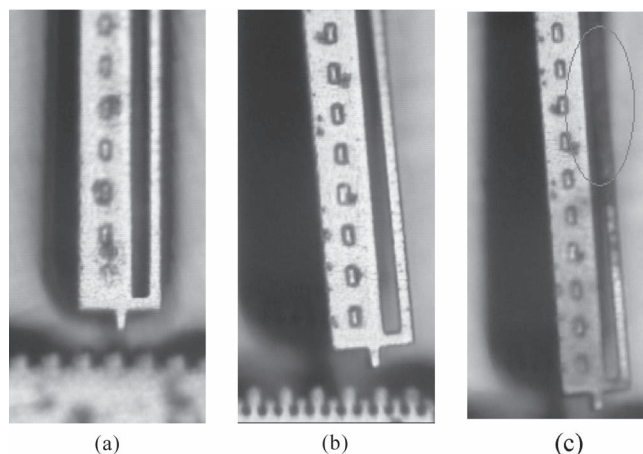


Fig. 7. Optical images of a thermal actuator show (a) the initial tip position and (b) the back bending after applying a pulse current of 54 mA and (c) burn-off followed by a high current of ~ 62 mA.

316 maximum backward displacement of $15 \mu\text{m}$ at $\sim 450^\circ\text{C}$, which
 317 is $\sim 75\%$ of the total forward displacement. The observed back-
 318 bending behavior with temperature for the D1 and D2 nickel
 319 microactuators is significantly different from that reported for
 320 silicon microactuators [6]. First, the average temperature of
 321 $\sim 160^\circ\text{C}$, which induces a measurable back bending for the
 322 nickel microactuators, is much lower than that of $\sim 660^\circ\text{C}$
 323 for the Si-based thermal actuators [6]. Second, while the back-
 324 bending displacement of the silicon actuators increases with
 325 power initially, it then remains at the maximum value as the
 326 power is further increased until the hot arm blows up [6]. Sil-
 327 icon is a relatively brittle material with a high melting tempera-
 328 ture, which can easily fracture or cleave along grain boundaries
 329 rather than softening at large stresses and high temperature.
 330 Further increases in temperature have been observed to lead
 331 to significant recrystallization and abnormal grain growth for
 332 polysilicon-based thermal actuators [10], [11]. Polysilicon re-
 333 crystallization to form large grain structures with crystal facets
 334 was observed at a temperature of 1100°C , which, while much
 335 lower than the melting temperature, roughly coincides with
 336 the temperature at which significant creep might be expected
 337 [9], [10]. Under a tensile stress at a high temperature, silicon
 338 plastic deformation is characterized by grain boundary separa-
 339 tion, internal cracking, and the formation of cavities [6], [10],
 340 rather than ductile necking.

341 Although nickel has a comparable melting temperature to
 342 silicon, it is ductile. The temperature to initiate plastic defor-
 343 mation in the nickel-based thermal actuators is much lower than
 344 that of comparable silicon microactuators. Since the estimated
 345 maximum temperature of the beam is $\sim 680^\circ\text{C}$, deformation
 346 by creep would seem to be responsible for the significant
 347 back-bending behavior of the nickel beams. Creep is thermally
 348 activated, so that both stress and temperature have profound
 349 effects on the process. Creep in metals can occur even at room
 350 temperature, provided that the stress level is sufficiently high
 351 [27]–[29]. This is significantly different from that of the silicon
 352 thermal actuators. As maximum temperature rises, the stress
 353 required to introduce creep in a nickel thermal actuator is much
 354 lower than that of a silicon actuator. Metals become much

more reactive at high temperatures, and metallic surfaces will
 be oxidized quickly at relatively low temperatures. However,
 the oxidation of surface seems unlikely to be instrumental in
 reducing the length of the hot arm as the volume of the material
 normally increases after oxidation, and so is unlikely to be the
 cause of the back bending of the nickel device.

The temperatures shown in Fig. 4 are the averages extracted
 from the variation of the resistances of the nickel microactua-
 tors D2. The maximum temperature is near the middle of the
 hot arm. A previous analysis based on the thermal conduction
 model indicated that the maximum temperature increase of the
 hot arm ΔT_{max} would be expected to be about 1.5 times the cal-
 culated average temperature increase ΔT_{ave} [21], [22]. Assum-
 ing an ambient temperature of 20°C , the average temperature of
 160°C shown in Fig. 7(b) corresponds to a maximum tempera-
 ture of $\sim 1.5 \times (160 - 20) + 20 = 230^\circ\text{C}$, i.e., close to 220°C
 suggested by Lee *et al.* [15]. The estimated average temperature
 of 450°C for severe degradation corresponds to a maximum
 temperature of $\sim 665^\circ\text{C}$, which should be high enough to
 induce significant creep, particularly at a large compressive
 stress. Furthermore, it is possible that these figures for average
 and maximum temperatures are underestimates as a result of
 the simplified model. The actual maximum temperature might
 exceed that estimated by $\sim 20\%$.

Device D1 showed smaller displacements in both forward
 displacement and back bending than those of the device D2,
 as shown in Figs. 2–4. It is believed to be caused by the thin Ni
 film, which is $3 \mu\text{m}$. When the film thickness is smaller than the
 width of the hot arm, a certain degree of out-of-plane buckling
 under thermal stress occurs. This will not introduce a plastic
 deformation, as it is well within the elastic state, but reduce the
 forward displacement and back bending.

In order to investigate the cause of back bending, the nickel
 microactuators were thermally stressed by passing a high cur-
 rent of 54 mA through the structure for 3 min, and the resulting
 changes in beam morphology were studied. The 54-mA current
 chosen for the experiment corresponds to the near-worst case
 of the back bending, as shown in Fig. 2. However, the average
 temperature was higher than that at 54 mA shown in Fig. 4, as
 the device was heated for 3 min, which is much longer than the
 0.1-s pulse measurement. The temperature increases, owing to
 the positive temperature coefficient of the resistivity. At the
 end of 3 min, the average temperature raised from $\sim 450^\circ\text{C}$ to
 $\sim 500^\circ\text{C}$, calculated from the increased resistance, correspond-
 ing to a maximum temperature of $\sim 1.5 \times (500 - 20) + 20 = 399$
 740°C . Fig. 8 shows the SEM images of a hot arm at various
 locations along its length after such a thermal treatment which
 illustrates some significant changes. Near the tip joint with the
 cold arm, the hot arm has retained the smooth surface finish
 of the original. At some distance from its ends, the surface of
 the hot arm becomes rougher and more rounded—evidence of
 plastic flow. Toward its mid-length, the beam cross section is
 significantly thinner, exhibiting a discernable neck. Near this
 position, on both sides of it, there is a significant accumulation
 or pileup of material. These changes in section, the general
 rounded appearance and lack of any preferred crystal facet,
 indicate that the metal has undergone a reflow process. As the
 melting temperature of nickel is 1455°C , it is unlikely that

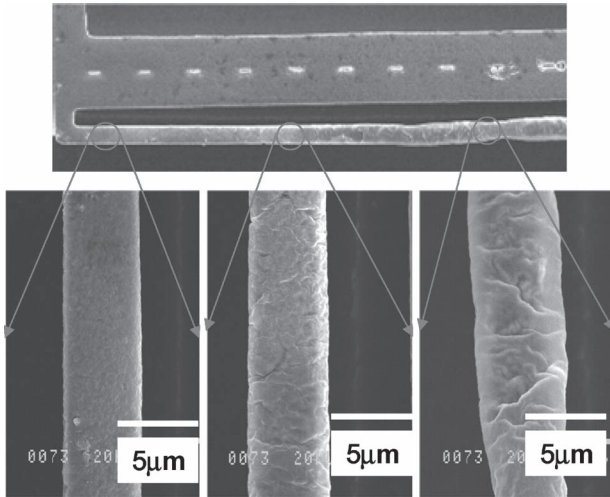


Fig. 8. SEM photographs of the hot arm in different places. The device had undergone heating by a current of 55 mA for 3 min. It showed the Ni pileup near the hotter places and necking at the hottest spot.

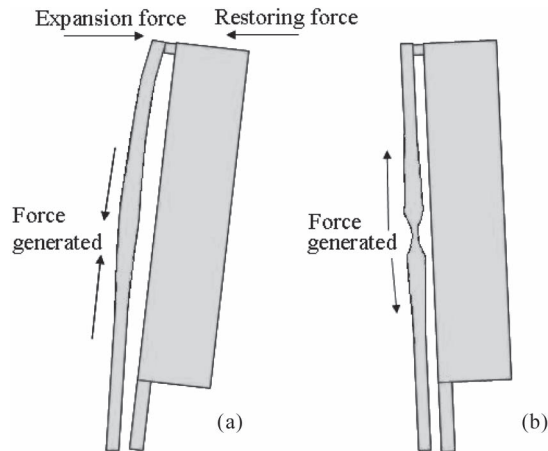


Fig. 9. (a) Schematic drawing of force acting on the hot arm when the current is applied; restoring force produces a compressive stress, leading to pileup of Ni. (b) When the current is removed, restoring force produces a tensile stress, leading to necking of the hot arm.

413 the reflow is caused by melting. It is believed that the material
414 pileup and reflow are associated with creep encouraged by
415 elevated temperatures and high stresses.

416 A dynamic model can thus be proposed for the plastic de-
417 formation of the nickel thermal microactuator shown schemati-
418 cally in Fig. 9. When the current is first applied, the differential
419 Joule heating of the thinner arm causes it to become hotter,
420 and thus, in an attempt to thermally lengthen by a greater
421 margin than the adjacent cold arm, this puts the material under a
422 compressive load. This compressive stress causes the material
423 to deform and pile up in compression, the raised temperature
424 accelerating this process. Nickel accumulates near the hottest
425 section forming the comparatively large folded structures visi-
426 ble at this section of the beam. It is this effective shortening of
427 the hot arm that is responsible for the subsequent back bending
428 of the actuator. Upon removing the current, the beam rotates
429 about its base as the force in the thinner arm changes from
430 compressive stress to tensile stress. This tensile stress tends to
431 elongate the shortened arm. Since the middle hottest section is

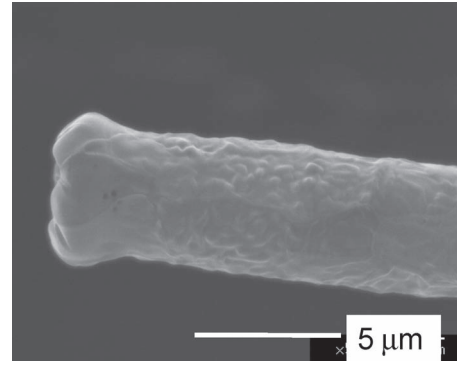


Fig. 10. SEM photograph of a blowup tip, showing a rounded structure which was caused by thermal runaway and melting.

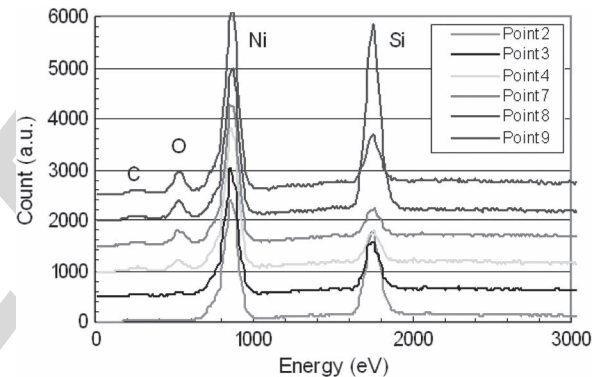


Fig. 11. EDX spectra from the surface of a hot arm after thermal stress at 55 mA for 3 min. As approaching the middle of the arm, the oxygen signal becomes much stronger.

the mechanically weakest, it is here that the extension occurs,
432 manifesting itself as the observed neck. 433

It is thus the combination of pileup and necking that is be-
434 lieved to be responsible for the decreases in forward and back-
435 bending displacements at $T_{ave} = T_0 + \Delta T_{ave} \Rightarrow 450 \text{ }^\circ\text{C}$, as
436 shown in Fig. 4. At a modest temperature, material pileup leads
437 to the shortening of the arm, causing the back bending and
438 reduction of forward displacement upon removing the current.
439 At $T_{ave} \Rightarrow 450 \text{ }^\circ\text{C}$, necking prevents further shortening of
440 the arm; hence, the back-bending displacement decreases as
441 the temperature increases further. Any further increase in the
442 current increases the temperature rapidly principally because of
443 the positive temperature coefficient of the resistivity of nickel,
444 rapidly leading to blowup of the hot arm. Fig. 10 shows a SEM
445 image of the tip of a failed arm, clearly showing the rounded
446 reflow structure. 447

D. Thermal Oxidation of the Beam 448

The surface of the nickel beams can be easily oxidized in
449 air at high temperatures, and this may significantly affect the
450 performance of these thermal actuators as a result of gradual
451 changes in their resistance and mechanical properties. EDX was
452 used to characterize the element concentration along the hot
453 arm of the device shown in Fig. 8, and the results are shown in
454 Fig. 11. Point 2 corresponds to a position where the hot and cold
455 arms are linked, and point 9 is close to the neck; intermediate
456

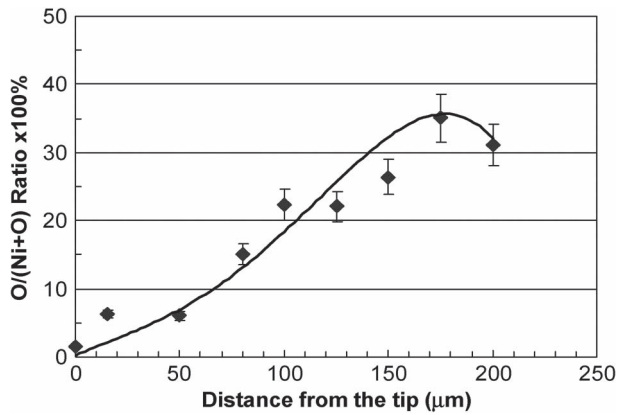


Fig. 12. Distribution of oxygen to Ni ratio along the hot arm. The oxygen content reaches the highest level at the middle of the hot arm.

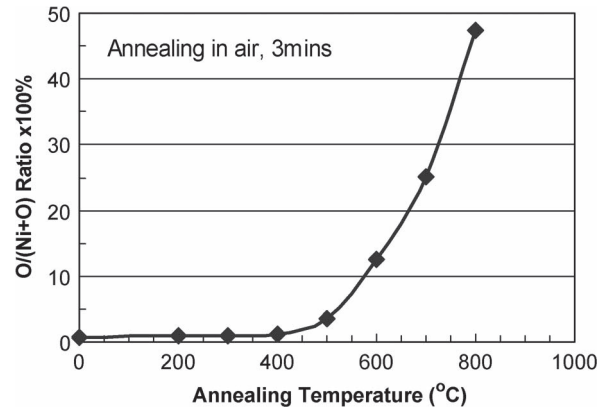


Fig. 13. Oxygen to nitrogen ratio as a function of annealing temperature for a Ni metal annealed in air for 3 min. The oxygen concentration increases rapidly as the temperature is over 450 °C and reaches ~36% at ~750 °C.

457 points are close to being equally spaced between them. The Si 458 signal is from the silicon substrate, as the scanning area of the 459 EDX measurements is wider than the hot arm width. Nickel 460 is the dominant peak with a small trace of carbon, which is 461 probably the residue from photoresist and plasma etching gases, 462 as well as some carbon absorbance from the ambient. The 463 oxygen concentration on the surface of the wide arm is typically 464 at the level of < 2% (near the detection limitation) and is 465 attributed to the thin native oxide and oxygen absorbance from 466 the ambient. Fig. 12 shows the oxygen concentration results 467 along the hot arm after the thermal overload treatment. The 468 oxygen concentration increases steadily from the arm edge and 469 reaches its highest value of ca. 36% roughly at the middle of the 470 hot arm. This clearly indicates that most of the hot arm surface 471 is oxidized after treatment with a 54-mA current maintained 472 for 3 min. The profile of the oxygen concentration along the 473 hot arm is also similar to the temperature profile obtained by 474 finite-element-analysis-based modeling [3], [25], implying that 475 the high temperature is directly responsible for the observed 476 oxidation.

477 For comparison, a series of electroplated Ni samples was also 478 annealed at temperatures from 200 °C to 800 °C for 3 min 479 in an air furnace (rapid thermal annealing), and their oxygen 480 concentration similarly investigated by EDX. The results are 481 shown in Fig. 13 as a function of the annealing temperature. 482 Up to 400 °C, the oxygen concentration remains below the 483 detection limitation but grows rapidly as the temperature in- 484 creases above 400 °C. The comparison of O/(O + Ni) ratios 485 along the hot arm of the actuator with those of the annealed 486 samples implies that the highest temperature of the hot arm was 487 around ~760 °C, which is in good agreement with the estimated 488 maximum temperature of 740 °C from the thermal conduction 489 model discussed before.

490 We also observed that the electrical resistance of the actuator 491 could be changed by the application of a current-driven thermal 492 cycle. This is illustrated by the data of Fig. 14 which shows 493 how the resistance of the device, measured at room temperature, 494 was influenced by the calculated average temperature during the 495 imposed thermal cycle. The resistance was measured at room 496 temperature by allowing the actuator to cool down prior to each 497 measurement, while the average temperature was calculated

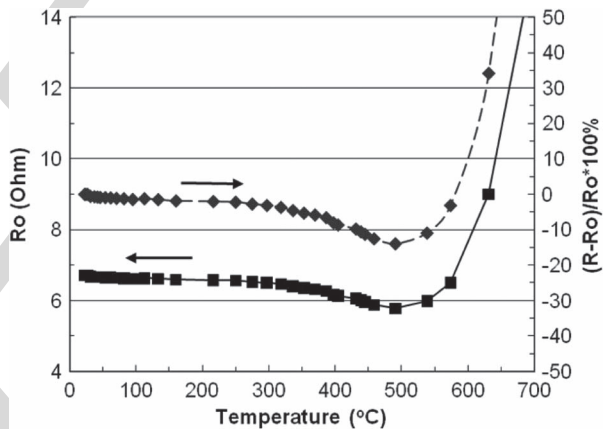


Fig. 14. Resistance of the thermal actuator as a function of average temperature measured. The resistance initially decreases, owing to annealing, and then increases rapidly when temperature exceeds 500 °C due to surface oxidation.

using the resistance measured when the current was on. As the 498 current increases, the average temperature rises. The resistance 499 of the device, determined principally by that of the hot arm, 500 initially slowly decreased with increasing temperatures up to 501 a value of ca. 500 °C, above which the resistance increased 502 rapidly, leading to thermal runaway and blowup. The initial 503 fall of the resistance with increasing average temperature is 504 believed to be caused by an annealing effect. Upon anneal- 505 ing at a modest temperature, an electroplated nickel structure 506 normally becomes dense with an increase in grain size and a 507 fall in resistance [30], [31]. Any further increase in average 508 temperature leads to severe surface oxidation, thus increasing 509 the resistance until the current path fails. The observed onset 510 temperature of ~500 °C for the resistance to increase rapidly 511 coincides with that of O/(Ni + O) ratio versus temperature pro- 512 file shown in Fig. 13. It is also clear that the resistance increases 513 dramatically after $T_{ave} \geq 500$ °C and reaches more than 150% 514 of its ambient value at 700 °C, at which the actuators become 515 sufficiently degraded to lead to a decreased displacement. It 516 can be concluded that both creep and the surface oxidation 517 at raised temperatures are responsible for the degradation in 518 displacement of the nickel thermal actuators.

520

IV. SUMMARY

521 U-shaped thermal microactuators were fabricated by a
522 single-mask process using electroplated nickel as the active
523 material. Their displacement and back bending have been char-
524 acterized, and their thermal degradation has been investigated
525 in detail. The results can be summarized as follows.

- 526 1) The nickel thermal actuators investigated delivered dis-
527 placements of up to 20 μm at an average temperature
528 of 450 $^{\circ}\text{C}$, which is much lower than those generally
529 required by Si-based microactuators. The displacement
530 strongly depends on the voltage amplitude of the pulse
531 signal used. The typical cutoff frequency for the thermal
532 actuators with a length of 400 μm was between 300 and
533 1000 Hz.
- 534 2) The phenomenon of back bending has been observed in
535 the chosen nickel-based thermal microactuators becom-
536 ing evident at average temperatures as low as 160 $^{\circ}\text{C}$: This
537 corresponds to a maximum temperature of 240 $^{\circ}\text{C}$ in the
538 hot beam. These values are much lower than what would
539 be expected in the case of silicon-based microactuators.
- 540 3) The magnitudes of both forward and back-bending dis-
541 placements have become larger with increases in tem-
542 perature up to 450 $^{\circ}\text{C}$, but then have been subsequently
543 decreased with temperature. Plastic deformation at high
544 temperature and surface oxidation of the nickel hot arm
545 are responsible for this phenomenon.
- 546 4) Reflow of the nickel has occurred under a compressive
547 stress at raised temperatures, which can cause the material
548 to pile up and thus make the beam locally larger in
549 cross section. Conversely, a tensile stress generated upon
550 the removal of the current can cause necking and local
551 thinning of the hot arm.
- 552 5) EDX characterization has revealed that the surface of
553 the hot arm is almost fully oxidized at a temperature
554 of ~ 750 $^{\circ}\text{C}$, leading to a rapid increase of the resistance
555 of the overall device.
- 556 6) Both plastic deformation and surface oxidation at raised
557 temperatures have been responsible for the reduction in
558 the available displacement of thermal actuators.

559

REFERENCES

560 [1] J. R. Reid, V. M. Bright, and J. H. Comtois, "Force measurements of
561 polysilicon thermal micro-actuators," *Proc. SPIE*, vol. 2882, pp. 296–306,
562 1996.

563 [2] T. Moulton and G. K. Ananthasuresh, "Micromechanical devices with
564 embedded electro-thermal-compliant actuation," *Sens. Actuators A, Phys.*,
565 vol. 90, no. 1/2, pp. 38–48, May 2001.

566 [3] Q. A. Huang and N. K. Lee, "Analysis and design of polysilicon thermal
567 flexure actuator," *J. Micromech. Microeng.*, vol. 9, no. 1, pp. 64–70,
568 Mar. 1999.

569 [4] R. L. Borwick, P. A. Stupar, and J. DeNatale, "A hybrid approach to low-
570 voltage MEMS switches," in *Proc. 12th Int. Conf. Transducer, Solid-State*
571 *Sens., Actuators Microsyst.*, 2003, vol. 1, pp. 859–862.

572 [5] J. H. Comtois and V. M. Bright, "Applications for surface-micromachined
573 polysilicon thermal actuators and arrays," *Sens. Actuators A, Phys.*,
574 vol. 58, no. 1, pp. 19–25, Jan. 1997.

575 [6] S. Deladi, G. Krijnen, and M. Elwenspoek, "Distinction of the irreversible
576 and reversible actuation regions of B-doped poly-Si based electrother-
577 mal actuators," *J. Micromech. Microeng.*, vol. 14, no. 9, pp. S31–S36,
578 Sep. 2004.

[7] J. Bagdahn and W. N. Sharp, "Fracture strength of polysilicon at stress 579
concentration," *J. Microelectromech. Syst.*, vol. 12, no. 3, pp. 302–312, 580
Jun. 2003.

[8] J. M. Maloney, D. S. Schreiber, and D. L. DeVoe, "Large-force elec- 582
trothermal liner micromotors," *J. Micromech. Microeng.*, vol. 14, no. 2, 583
pp. 226–234, Feb. 2004.

[9] R. A. Conant and R. S. Muller, "Cyclic fatigue testing of surface- 585
micromachined thermal actuators," in *Proc. ASME*, 1998, vol. DSC-V.66, 586
pp. 273–277.

[10] S. Nakao, T. Ando, M. Shikeda, and K. Sato, "Mechanical proper- 588
ties of a micron-sized SCS film in a high-temperature environment," *J.* 589
Micromech. Microeng., vol. 16, no. 4, pp. 715–720, Apr. 2006.

[11] A. Tuck, A. Jungen, A. Geisberger, M. Ellis, and G. Skidmore, "A study 591
of creep in polysilicon MEMS devices," *J. Eng. Mater. Technol.*, vol. 127, 592
no. 1, pp. 90–96, Jan. 2005.

[12] J. K. Luo, J. H. He, A. J. Flewitt, D. F. Moore, S. M. Spearing, N. A. Fleck, 594
and W. I. Milne, "Development of all metal electro-thermal actuators 595
and its applications," *J. Microlith. Microfab. Microsyst.*, vol. 4, no. 2, 596
p. 023 012-1, 2005.

[13] P. M. Zavracky, S. Majumder, and N. E. McGruer, "Micromechanical 598
switches fabricated using nickel surface micromachining," *J. Micro-* 599
electromech. Syst., vol. 6, no. 1, pp. 3–9, Mar. 1997.

[14] I. Schiele, J. Huber, B. Hillerich, and F. Kozlowski, "Surface- 601
micromachined electrostatic microrelay," *Sens. Actuators A, Phys.*, 602
vol. 66, no. 1–3, pp. 345–354, Apr. 1998.

[15] J. S. Lee, S. D. Park, A. K. Nallani, G. S. Lee, and J. B. Lee, "Sub-micron 604
metallic electrothermal actuators," *J. Micromech. Microeng.*, vol. 15, 605
no. 2, pp. 322–327, Feb. 2005.

[16] D. A. Fanner and R. A. F. Hammond, "The properties of nickel 607
electrodeposited from a sulphamate bath," *Trans. Inst. Met. Finish.*, 608
vol. 36, pp. 32–42, 1959.

[17] L. S. Stephens, K. W. Kelly, S. Simhadri, A. B. McCandless, and 610
E. I. Meletis, "Mechanical property evaluation and failure analysis of 611
cantilevered LIGA nickel microposts," *J. Microelectromech. Syst.*, vol. 10, 612
no. 3, pp. 347–359, Sep. 2001.

[18] F. Wang, R. Cheng, and X. Li, "MEMS vertical probe cards with ultra 614
densely arrayed metal probes for wafer-level IC testing," *J. Microelectro-* 615
mech. Syst., vol. 18, no. 4, pp. 933–941, Aug. 2009.

[19] R. V. Shenoy and M. Datta, "Effect of mask wall angle on shape evolution 617
during through-mask electrochemical micromachining," *J. Electrochem.* 618
Soc., vol. 143, no. 2, pp. 544–552, 1996.

[20] J. K. Luo, D. P. Chu, A. J. Flewitt, S. M. Spearing, N. A. Fleck, and 620
W. I. Milne, "Uniformity control of Ni thin film microstructure deposited 621
by through-mask plating," *J. Electrochem. Soc.*, vol. 152, no. 1, pp. C36– 622
C41, 2005.

[21] J. K. Luo, A. J. Flewitt, S. M. Spearing, N. A. Fleck, and W. I. Milne, 624
"Comparison of microtweezers based on three lateral thermal actuator 625
configurations," *J. Micromech. Microeng.*, vol. 15, no. 6, pp. 1294–1302, 626
Jun. 2005.

[22] J. K. Luo, A. J. Flewitt, S. M. Spearing, N. A. Fleck, and W. I. Milne, 628
"Three types of planar structure microspring electro-thermal actuators 629
with insulating beam constraint," *J. Micromech. Microeng.*, vol. 15, no. 8, 630
pp. 1527–1535, Aug. 2005.

[23] J. K. Luo, M. Pritschow, A. J. Flewitt, S. M. Spearing, N. A. Fleck, and 632
W. I. Milne, "Effects of process conditions on properties of electro- 633
plated Ni thin films for microsystems applications," *J. Electrochem. Soc.*, 634
vol. 153, no. 10, pp. D155–D161, 2005.

[24] E. T. Enikov and K. Lazarov, "PCB-integrated metallic thermal micro- 636
actuators," *Sens. Actuators A, Phys.*, vol. 105, no. 1, pp. 76–82, Jun. 2003. 637

[25] R. Hickey, D. Sameoto, T. Hubbard, and M. Kujath, "Time and frequency 638
response of two-arm micromachined thermal actuators," *J. Micromech.* 639
Microeng., vol. 13, no. 1, pp. 40–46, Jan. 2003.

[26] R. Kickey, M. Kujath, and T. Hubbard, "Heat transfer analysis and opti- 641
mization of two-beam microelectromechanical thermal actuators," *J. Vac.* 642
Sci. Technol. A, Vac. Surf. Films, vol. 20, no. 3, pp. 971–974, May 2002. 643

[27] Z. Budrovic, H. V. Swygenhoven, P. M. Derlet, S. V. Petegem, and 644
B. Schmitt, "Plastic deformation with reversible peak broadening in 645
nanocrystalline nickel," *Science*, vol. 304, no. 5668, pp. 273–276, 646
Apr. 2004.

[28] X. Z. Liao, A. R. Kilmametov, R. Z. Valiev, H. Gao, X. Li, 648
A. K. Mukherjee, J. F. Binger, and Y. T. Zhu, "High-pressure torsion- 649
induced grain growth in electrodeposited nanocrystalline Ni," *Appl. Phys.* 650
Let., vol. 88, no. 21, p. 021 909, May 2006.

[29] G. J. Fan, Y. D. Wang, L. F. Fu, H. Choo, P. K. Liaw, Y. Ren, and 652
W. N. D. Browning, "Orientation-dependent grain growth in a bulk nanocryst- 653
talline alloy during the uniaxial compressive deformation," *Appl. Phys.* 654
Let., vol. 88, no. 17, p. 171 914, Apr. 2006. 655

AQ3

656 [30] S. C. Chang, J. M. Shieh, B. T. Dai, M. S. Feng, and Y. H. Li, "The effect
657 of plating current density on self-annealing behaviours of electroplated
658 copper film," *J. Electrochem. Soc.*, vol. 149, no. 9, pp. G535–G538, 2002.
659 [31] W. H. Safranek, "Structure and property relationship for bulk electrode-
660 posits," *J. Vac. Sci. Technol.*, vol. 11, no. 4, pp. 765–770, 1974.

Y. Q. Fu, photograph and biography not available at the time of publication. 662 **AQ5**

J. A. Williams, photograph and biography not available at the time of 663 **AQ6**
publication. 664

AQ4 661 **J. K. Luo**, photograph and biography not available at the time of publication.

W. I. Milne, photograph and biography not available at the time of publication. 665 **AQ7**

IEEE
Proof

AUTHOR QUERIES

AUTHOR PLEASE ANSWER ALL QUERIES

AQ1 = The acronym “EPSRC” was defined as “Engineering and Physical Sciences Research Council.”
Please check if correct.

AQ2 = The acronym “MEMS” was defined as “microelectromechanical system.” Please check if correct.

AQ3 = Please provide complete title of proceedings in Ref. [9].

AQ4 = Please provide photograph and biography of author J. K. Luo.

AQ5 = Please provide photograph and biography of author Y. Q. Fu.

AQ6 = Please provide photograph and biography of author J. A. Williams.

AQ7 = Please provide photograph and biography of author W. I. Milne.

END OF ALL QUERIES

IEEE
Proof